

# Stability of cosmological detonation fronts

Ariel Mégevand\* and Federico Agustín Membiela†

*IFIMAR (CONICET-UNMdP) and*

*Departamento de Física, Facultad de Ciencias Exactas y Naturales,  
UNMdP, Deán Funes 3350, (7600) Mar del Plata, Argentina*

The steady state propagation of a phase transition front is classified, according to hydrodynamics, as a deflagration or a detonation, depending on its velocity with respect to the fluid. These propagation modes are further divided into three types, namely, weak, Jouguet, and strong solutions, according to their disturbance of the fluid. However, some of these hydrodynamic modes will not be realized in a phase transition. One particular cause is the presence of instabilities. In this work we study the linear stability of weak detonations, which are generally believed to be stable. After discussing in detail the weak detonation solution, we consider small perturbations of the interface and the fluid configuration. When the balance between the driving and friction forces is taken into account, it turns out that there are actually two different kinds of weak detonations, which behave very differently as functions of the parameters. We show that the branch of stronger weak detonations are unstable, except very close to the Jouguet point, where our approach breaks down.

## I. INTRODUCTION

In a cosmological first-order phase transition, bubbles of the stable phase nucleate and expand in the supercooled metastable phase. The motion and collisions of bubble walls are associated with the formation of cosmological remnants, such as gravitational waves [1], magnetic fields [2], topological defects [3], a baryon asymmetry [4], or baryon inhomogeneities [5–7]. The propagation of bubble walls is driven essentially by the pressure difference between the two phases, but is significantly affected by hydrodynamics [8] (for recent studies, see [9–13]). Indeed, besides stirring the fluid, these phase transition fronts reheat the plasma, due to the release of latent heat. The back-reaction of such disturbances hinders the wall motion. In addition, the microscopic interaction of particles of the plasma with the wall causes, at the macroscopic level, a friction force [14–17]. In general, after a time which is much shorter than the total duration of the phase transition, the wall reaches a steady state with constant velocity (however, the wall may also run away [15]).

As a consequence of nonlinear hydrodynamics, different kinds of stationary solutions exist. Thus, the phase transition front may propagate, in principle, either as a weak, Jouguet, or strong deflagration, as well as a weak, Jouguet, or strong detonation. The latter, however, is not possible, since its fluid profile cannot fulfil the boundary conditions. These various propagation modes coexist in some ranges of parameters, and it is not easy to determine,

---

\*Member of CONICET, Argentina; megevand@mdp.edu.ar

†Fellow of CONICET, Argentina; membiela@mdp.edu.ar

in general, which of them will be actually reached in the phase transition. It will certainly depend on the initial and boundary conditions during the early transitory stage.

In the literature, the wall velocity is often given convenient values or left as a free parameter. For instance, slow-moving weak deflagrations are often assumed for baryogenesis, while fast-moving detonations are assumed for gravity-wave generation. In the latter case, a Jouguet detonation is often assumed. This solution corresponds to the lower bound for the detonation velocity. The choice of this particular solution avoids calculating the wall velocity, which would involve considering the balance of the driving and friction forces. This assumption is motivated by the case of chemical burning, where weak detonations are forbidden [18]. However, a phase transition is qualitatively different from chemical burning, and weak detonations are possible in addition to Jouguet detonations [19].

Even when a complete calculation of the wall velocity is performed, there still remains the problem of the existence of multiple solutions (for a recent discussion, see [13]). Besides the coexistence of the aforementioned kinds of solutions, a calculation of the wall velocity may give double-valued solutions of a given kind. In particular, for the weak detonation case, there are in general two branches. One of these branches consists of higher velocity solutions, which are hydrodynamically weaker (they cause smaller disturbances of the fluid). These solutions approach the speed of light for low enough friction or high enough supercooling. The other branch of weak detonations consists of stronger solutions with lower velocities, and ends at the Jouguet point. These detonations behave unphysically as a function of the parameters. Therefore, weak detonations might be divided into “weaker” weak detonations and “stronger” weak detonations.

An important issue is, thus, to determine the actual propagation mode for a given set of parameters. A stability analysis provides a useful tool to determine the final state of the wall motion, since not all of the possible hydrodynamic solutions turn out to be stable. For instance, it is known that strong deflagrations are generally unstable, and that weak deflagrations are unstable in certain ranges of parameters [20, 21]. The case of detonations is less clear.

In the cosmological context, the stability of weak detonations was first discussed by Huet et al. [20]. The standard approach is to consider small perturbations of the fluid variables on each side of the wall, together with small deformations of the latter, which is assumed to be infinitely thin [22, 23]. The fluid perturbations on the two phases are linked by junction conditions at the interface. In the case of detonations, the fluid enters the wall supersonically (in the reference frame of the latter). As a consequence, fluid perturbations cannot evolve in front of the wall. This fact lead Huet et al. to conclude that perturbations cannot grow at all, and weak detonations are always stable. However, numerical calculations of the time evolution of the wall-fluid system seem to indicate that configurations belonging to the “stronger” branch of weak detonations are unstable [24].

In fact, as noted by Abney [25], the conclusion of Ref. [20] is incorrect, as fluid perturbations may vanish in front of the wall and not behind it (and fulfil the junction conditions). Such perturbations, which were not considered in [20], may be unstable. Unfortunately, Abney (and later Rezzola [26]) considered only Jouguet and strong detonations. As already mentioned, the latter are not possible in a phase transition. Moreover, even in the case of Jouguet detonations, the treatment of Refs. [25, 26] is not valid. In the first place, an equation for the interface (depending on the driving and friction forces) was not considered in these works, even though its importance had been already pointed out by Huet et al. [20]. Most important, the treatment considers perturbations around a solution of constant fluid

velocity  $v$  and temperature  $T$ , whereas the fluid profile for a Jouguet detonation is that of a rarefaction wave behind the wall, with  $v$  and  $T$  varying in space and time.

In this paper we shall consider the hydrodynamic stability of detonation fronts in a cosmological phase transition. We shall consider only weak detonations. Unfortunately, for the case of Jouguet detonations, the fact that the fluid profiles are not constant behind the wall makes the treatment too involved. For the same reason, our approach will break down for weak detonations which are very close to the Jouguet point. Except in this limit, we will show that the lower velocity branch of weak detonations is unstable under linear perturbations at all wavelengths. Our approach is essentially the same we used in Ref. [21] for the case of weak deflagrations, and we shall refer to that work for some details. Due to the vanishing of perturbations in the metastable phase, the treatment of detonations turns out to be much simpler than that of deflagrations. This will allow us to obtain analytical and model-independent results.

The plan of the paper is the following. Before performing the stability analysis, we devote the next section to a detailed discussion on the structure of weak detonations. We also consider the coexistence with runaway solutions. In Sec. III we solve the equations for the linear perturbations of the wall-fluid system, and in Sec. IV we discuss in detail the velocity intervals corresponding to unstable solutions and to the validity of our approach. We also discuss some implications of our results for a cosmological phase transition. Our conclusions are summarized in Sec. V.

## II. DETONATION FRONTS IN A PHASE TRANSITION

For a given theory, a phase transition may occur if the free energy depends on a scalar field  $\phi$  which acts as an order parameter [27]. Thus, if the free energy density  $\mathcal{F}(\phi, T)$  has a minimum  $\phi_+$  at high temperature, and a different minimum  $\phi_-$  at low temperature, we have two different phases. Each phase will be described by a free energy density  $\mathcal{F}_\pm(T) = \mathcal{F}(\phi_\pm, T)$ . Indeed, all the thermodynamical quantities in each phase can be derived from the functions  $\mathcal{F}_\pm(T)$ . Such a relation between thermodynamical quantities is known as an equation of state (EOS). For instance, the pressure is given by  $p = -\mathcal{F}(T)$ , the entropy density by  $s = dp/dT$ , the enthalpy density by  $w = Ts$ , and the energy density by  $e = Ts - p$ .

If the phase transition is first-order, there is a range of temperatures at which the two minima  $\phi_\pm$  coexist, separated by a barrier. The critical temperature  $T_c$  is that at which  $\phi_+$  and  $\phi_-$  have the same free energy, i.e.,  $T_c$  is defined by  $\mathcal{F}_+(T_c) = \mathcal{F}_-(T_c)$ . Some quantities (e.g., the energy and the entropy) are discontinuous at  $T = T_c$ . The latent heat is defined as the energy density discontinuity at  $T = T_c$ , and is given by  $L = T_c[\mathcal{F}'_-(T_c) - \mathcal{F}'_+(T_c)]$ .

In the early universe, the system is initially in the high-temperature phase. As the temperature descends below  $T_c$ , the  $+$  phase becomes metastable, but the system remains in this supercooled phase due to the free-energy barrier between minima (see, e.g., [28–30]). Finally, at some temperature  $T_N < T_c$ , bubbles of the stable low-temperature phase begin to nucleate and grow, until they fill all space (for reviews on phase transition dynamics, see, e.g., [31]). The expectation value of the field takes the value  $\phi_-$  inside the bubble and the value  $\phi_+$  outside it. Thus, the bubble can be seen as a classical-field configuration. The walls of these bubbles interact with the particles of the plasma. At the same time, the bubble walls are phase transition fronts, at which latent heat is released.

Macroscopically, we can describe the field-fluid system by considering the conservation of the stress tensor, together with a finite-temperature equation for the field. These equations

can be written in the form

$$\partial_\mu \left( -T \frac{\partial \mathcal{F}}{\partial T} u^\mu u^\nu + g^{\mu\nu} \mathcal{F} \right) + \partial_\mu \partial^\mu \phi \partial^\nu \phi = 0, \quad (1)$$

$$\partial_\mu \partial^\mu \phi + \frac{\partial \mathcal{F}}{\partial \phi} + \frac{\tilde{\eta} u^\mu \partial_\mu \phi}{\sqrt{1 + (\tilde{\lambda} u^\mu \partial_\mu \phi)^2}} = 0, \quad (2)$$

with  $u^\mu = (\gamma, \gamma \mathbf{v})$  the four velocity of the fluid and  $g^{\mu\nu}$  the Minkowsky metric tensor. Notice that the terms in parenthesis in Eq. (1) correspond to the familiar stress tensor of the relativistic fluid,  $w u^\mu u^\nu - p g^{\mu\nu}$ . The last term in this equation gives the transfer of energy between the plasma and the field. The field is governed by Eq. (2), where we have included, as is customary, a phenomenological damping term proportional to  $u^\mu \partial_\mu \phi$ . This term will give the friction force between the wall and the plasma. The particular form used in Eq. (2) was proposed in Ref. [17] in order to account for the saturation of the friction force at ultra-relativistic velocities [15]. The coefficients  $\tilde{\eta}$  and  $\tilde{\lambda}$  can be obtained from microphysics calculations (in the general case,  $\tilde{\eta}$  and  $\tilde{\lambda}$  may depend on the field  $\phi$ ). The coefficient  $\tilde{\eta}$  will dominate for non-relativistic fluid velocities, whereas the coefficient  $\tilde{\lambda}$  will dominate the ultra-relativistic behavior. Similar damping terms (with a single parameter) have been considered in Refs. [10, 16].

For the distance scales associated to the wall motion and hydrodynamic profiles, the bubble wall can be regarded as an infinitely thin interface. Due to the friction with the plasma, this interface will in general reach a terminal velocity. However, due to the saturation of the friction force at ultra-relativistic velocities, a state of continuous acceleration [15] also exists. Besides, as we have already mentioned, stationary solutions may be unstable. We shall now consider the stationary motion of a planar interface, focusing on the detonation case, and in the next section we shall study perturbations of this configuration.

### A. Hydrodynamic solutions

Let us consider a planar wall moving towards the positive  $z$  axis. Due to the planar symmetry, the fluid velocity is perpendicular to the wall (see Fig. 1). The fluid velocity and the temperature are different on each side of the wall. The relation between these values can be obtained by integrating Eq. (1) across the interface. In the reference frame of the wall, we obtain

$$w_- v_- \gamma_-^2 = w_+ v_+ \gamma_+^2, \quad (3)$$

$$w_- v_-^2 \gamma_-^2 + p_- = w_+ v_+^2 \gamma_+^2 + p_+, \quad (4)$$

where  $v$  is the  $z$  component of the fluid velocity, and  $+$  and  $-$  signs refer to variables just in front and just behind the wall, respectively. Notice that in this frame we have  $v_\pm < 0$ . If the equation of state is known, Eqs. (3-4) can be used to obtain the velocity and temperature of the outgoing flow as functions of the incoming flow variables. Nevertheless, some general features of these hydrodynamic relations do not depend on the EOS.

In the first place, it is easy to see that we have two branches of hydrodynamic solutions. Indeed, from Eqs. (3-4) we may write

$$\frac{v_+ - v_-}{v_+} = \frac{p_- - p_+}{w_+ \gamma_+^2 v_+^2}. \quad (5)$$

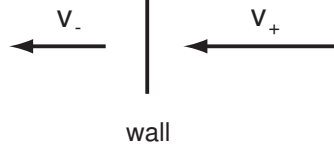


FIG. 1: Sketch of a detonation in the wall frame.

Therefore, we see that, for given values of  $v_+$  and  $T_+$ , we will have in general two solutions for the outgoing flow. One of them with<sup>1</sup>  $|v_-| < |v_+|$  and  $p_+ < p_-$ , called *detonation*, and the other with  $|v_-| > |v_+|$  and  $p_+ > p_-$ , called *deflagration* (the sketch of Fig. 1 corresponds to a detonation configuration).

In the second place, notice that *variations* of thermodynamical quantities are generally related by the speed of sound, which is given by  $c_s^2 \equiv dp/de$ . We have, in particular,

$$dp = dw/(1 + c_s^{-2}). \quad (6)$$

Therefore, differentiating Eqs. (3-4) we may gather all the information on the EOS in this single parameter. Let us regard the temperature  $T_+$  in front of the wall as a boundary condition (this is the case if the incoming flow is supersonic), and consider the dependence of  $v_-$  and  $T_-$  on  $v_+$ . We have

$$\left( v_-^2 \gamma_-^2 + \frac{c_{s-}^2}{1 + c_{s-}^2} \right) dw_- + 2w_+ v_+ \gamma_+^2 \gamma_-^2 dv_- = 2w_+ v_+ \gamma_+^4 dv_+, \quad (7)$$

$$v_- \gamma_-^2 dw_- + w_+ \gamma_+^2 \gamma_-^2 \frac{v_+}{v_-} (1 + v_-^2) dv_- = w_+ \gamma_+^4 (1 + v_+^2) dv_+, \quad (8)$$

where we have used the relations  $d(v^2 \gamma^2) = 2v \gamma^4 dv$ ,  $d(v \gamma^2) = \gamma^4 (1 + v^2) dv$ . Combining Eqs. (7-8), we obtain

$$\left. \frac{\partial v_-}{\partial v_+} \right|_{T_+} = \frac{\gamma_+^2}{\gamma_-^2} + \frac{\gamma_+^2 (v_-^2 + c_{s-}^2) (1 - v_+ v_-)}{v_-^2 - c_{s-}^2} \frac{v_+ - v_-}{v_+}, \quad (9)$$

$$\frac{1}{w_-} \left. \frac{\partial w_-}{\partial v_+} \right|_{T_+} = - \frac{2v_- \gamma_-^2 \gamma_+^2 (1 + c_{s-}^2) (1 - v_+ v_-)}{v_-^2 - c_{s-}^2} \frac{v_+ - v_-}{v_+}. \quad (10)$$

Notice that these equations do not depend on the sign of  $v_{\pm}$ , and are valid for a wall propagating towards the negative  $z$  axis as well.

It is evident that the speed of sound in the  $-$  phase plays a relevant role in Eqs. (9-10). For instance, the inverse of the derivative in Eq. (9) vanishes at this point, which means that the curve of  $v_+$  as a function of  $v_-$  has an extremum. Thus, the case  $|v_-| = c_{s-}$  separates two different behaviors, namely,  $v_+$  growing with  $v_-$ , or  $v_+$  decreasing with  $v_-$ . The former are called weak solutions and the latter are called strong solutions. The point  $|v_-| = c_{s-}$  is called the Jouguet point. The extremum of  $v_+$  vs.  $v_-$  at the Jouguet point will be either a maximum or a minimum, depending on the sign of  $(v_+ - v_-)/v_+$ . Thus, for detonations we have a minimum, whereas for deflagrations we have a maximum (see Fig. 2).

<sup>1</sup> Notice that  $(v_+ - v_-)/v_+ = (|v_+| - |v_-|)/|v_+|$ .

Physically, we know that there must be solutions with low values of  $v_-$  and  $v_+$ , corresponding to a slow wall. In the limit of a vanishingly small wall velocity, we must have  $v_- = v_+ = 0$ , while if the wall velocity is small but nonvanishing, both  $v_-$  and  $v_+$  will be nonvanishing (and will have the same sign). Hence, these solutions correspond to the *weak* part of a curve (i.e.,  $\partial v_+/\partial v_- > 0$ ). If we increase further the velocity, we will reach the Jouguet point  $|v_-| = c_{s-}$ , where, according to the above,  $|v_+|$  has an extremum. In this case, the extremum must be a maximum, and  $|v_+|$  will decrease for  $|v_-| > c_{s-}$  (strong solutions). Thus, we are in a deflagration curve.

On the other hand, there must also be solutions with  $v_- \approx v_+ \approx 1$ , corresponding to a very fast moving wall. As the wall velocity decreases from the limit  $v_w = 1$ , both  $|v_+|$  and  $|v_-|$  will decrease. Therefore, we are again in the weak part of a curve. This curve must have a minimum at the Jouguet point  $|v_-| = c_{s-}$  and, thus, corresponds to detonation solutions.

Thus, we see that, for detonations, the incoming flow is supersonic, whereas for deflagrations the incoming flow is subsonic. Notice also that weak solutions correspond to smaller values of  $v_+ - v_-$  than strong solutions and, thus, to weaker disturbances of the fluid. For weak deflagrations, the wall velocity is subsonic with respect to the fluid on both sides of it, whereas for weak detonations the wall velocity is supersonic with respect to the fluid on both sides.

We may obtain the form of the detonation and deflagration curves if we integrate Eqs. (9-10), although some information will be lost with respect to Eqs. (3-4) (namely, there will be undetermined integration constants). In general,  $c_{s-}$  is a function of  $w_-$ , and the two derivatives in (9-10) cannot be integrated independently. Nevertheless, if we neglect the variation of the speed of sound, Eq. (9) can be integrated alone. In Fig. 2 we show the result<sup>2</sup> for the case  $c_{s-} = 1/\sqrt{3}$  (corresponding to an ultra-relativistic gas). We have arbitrarily chosen two conditions to determine the integration constant, corresponding to detonations and deflagrations (for a specific EOS, the two values of  $v_+$  for a given  $v_-$  will be determined as functions of  $T_+$ ). The result is similar for any constant value of  $c_{s-}$ . In the general case the curves are also similar, but  $c_{s-}$  may be different in each curve, as it depends on the temperature.

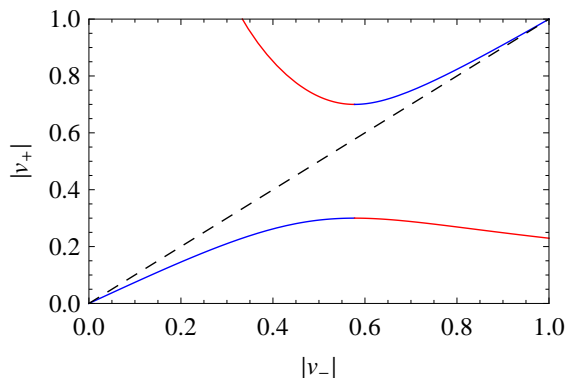


FIG. 2: The fluid velocities in the rest frame of the wall for fixed  $T_+$ , obtained from Eq. (9) for  $c_{s-} = 1/\sqrt{3}$ , with conditions  $v_+(c_{s-}) = 0.3$  (lower curve) and  $v_+(c_{s-}) = 0.7$  (upper curve). Blue lines indicate weak solutions and red lines indicate strong solutions. The dashed line indicates the value of  $v_+ = v_-$ .

<sup>2</sup> We actually integrated the inverse of Eq. (9), i.e.,  $\partial v_+/\partial v_-$ .

## B. Fluid profiles

Away from the wall, the field is a constant and Eq. (1) gives the conservation of energy and momentum for the fluid, i.e.,  $\partial_\mu(wu^\mu u^\nu - pg^{\mu\nu}) = 0$ . Using Eq. (6), we may obtain again equations which depend only on the parameter  $c_s$  [22]. Besides, the absence of a distance scale in these equations justifies to assume the *similarity condition*, namely, that the solution will depend only on the variable  $\xi = z/t$ . In the planar case, one obtains very simple equations for  $v(\xi)$  and  $w(\xi)$  (see e.g. [11]). The solutions are<sup>3</sup>

$$v(\xi) = \text{constant} \quad (11)$$

and the rarefaction wave

$$v_{\text{rar}}(\xi) = \frac{\xi - c_s}{1 - \xi c_s}. \quad (12)$$

Notice that there is no integration constant in Eq. (12). The corresponding solutions for the thermodynamical variables are given by

$$w(\xi) = \text{constant} \quad (13)$$

and by

$$\frac{c_s}{1 + c_s^2} \frac{dw}{w} = \gamma^2 dv. \quad (14)$$

The latter is trivially integrated in the case of constant  $c_s$ .

The boundary conditions are, in the reference frame of the bubble center, that the fluid velocity vanishes far behind the wall (i.e., at the center of the bubble) and far in front of the wall (where the fluid is still unperturbed). Therefore, in the wall frame, the fluid velocity far in front and far behind the wall must be given by  $v = -v_w$ . The boundary condition for the temperature is that its value far in front of the wall is given by the nucleation temperature  $T_N$ .

It is not difficult to construct the fluid velocity and temperature profiles from the similarity solutions, using the boundary conditions and the matching conditions at the wall. Let us consider the detonation case. As we have seen, the incoming flow is supersonic and, hence, has not received any information from the wall. As a consequence, the boundary condition gives  $v_+ = -v_w$ . As we have seen, for a detonation we have  $|v_-| < |v_+|$  (hence,  $v_- > v_+$ ), which means that the fluid in the  $-$  phase is dragged by the wall. Behind the wall, the velocity must descend continuously<sup>4</sup> from its value at the wall,  $v_-$ , to the value at the bubble center,  $-v_w$ . To achieve this, we must use the rarefaction solution (12) as well as constant solutions  $v = v_+$  and  $v = v_-$ , as shown in the left panel of Fig. 3<sup>5</sup>. In the wall frame, the wall is at  $\xi_w = 0$ . The rarefaction solution matches the value  $v_-$  at

$$\xi_0 = (c_{s-} + v_-)/(1 + c_{s-}v_-) \quad (15)$$

<sup>3</sup> In fact, there is also a solution  $v = (\xi + c_s)/(1 + \xi c_s)$ , but this solution will not fulfil the matching and boundary conditions [11].

<sup>4</sup> Entropy considerations show that we cannot have a discontinuity with  $v$  increasing in the direction of the front propagation (for details, see e.g. [11]).

<sup>5</sup> In the figure we have chosen arbitrarily the values of  $v_+$  and  $v_-$ . For a given EOS, these values will be given by the matching conditions.

and the value  $v_+$  at

$$\xi_c = (-v_w + c_{s-})/(1 - v_w c_{s-}) \quad (16)$$

In the frame of the bubble center, the fluid velocity vanishes at this latter point, which moves with velocity  $c_{s-}$ . The temperature profile is qualitatively similar to the velocity profile. In front of the wall we have a constant temperature  $T_+ = T_N$ . Behind the wall the fluid is reheated to a temperature  $T_-$ , which then descends along the rarefaction wave to a final value  $T_f \simeq T_N$ .

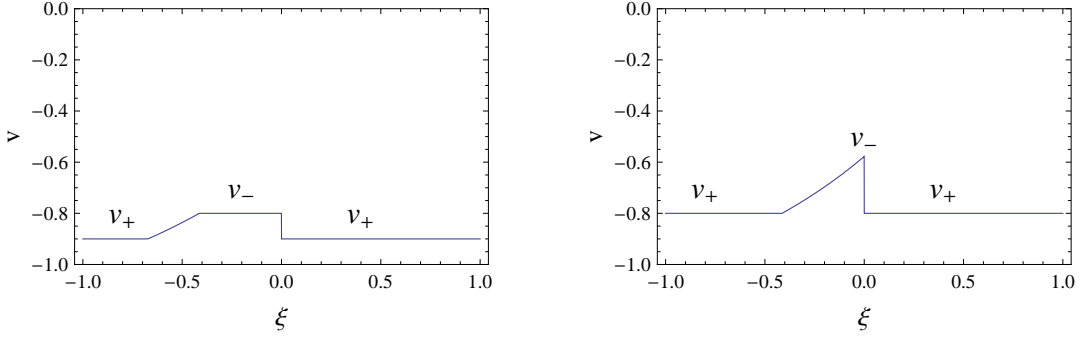


FIG. 3: The fluid velocity profile for  $c_{s-} = 1/\sqrt{3}$ , in the reference frame of the bubble wall. Left panel: a weak detonation ( $v_+ = -0.9$ ,  $v_- = -0.8$ ). Right panel: a Jouguet detonation ( $v_+ = -0.8$ ,  $v_- = -c_{s-}$ ).

Notice that this profile is only possible for weak or Jouguet detonations (i.e., for  $v_- \leq -c_{s-}$ ). In fact, at the Jouguet point we have  $\xi_0 = \xi_w = 0$ , and the region of constant velocity  $v_-$  disappears (right panel of Fig. 3). A strong detonation would require  $\xi_0 > \xi_w$ , and the fluid profile cannot be constructed. Therefore, strong detonations are not possible.

Strong deflagration profiles can be constructed, but are unstable (see [21] for details). For a weak deflagration, both  $v_+$  and  $v_-$  are subsonic, and the rarefaction solution  $v_{\text{rar}}(\xi)$  cannot be accommodated in the velocity profile. Therefore, the fluid velocity takes the constant value  $v = v_-$  everywhere behind the wall. According to the boundary condition at the bubble center, we thus have  $v_- = -v_w$ . For a deflagration we have  $|v_+| < |v_-|$ , which means that the fluid is pushed forward in front of the wall. Hence, we have a constant solution  $v = v_+ > v_-$  up to a certain point  $\xi_{\text{sh}}$ , where the velocity must descend abruptly to take the boundary value  $v = -v_w = v_-$ . Such a discontinuity without a change of phase is called a shock front. At the shock discontinuity, Eqs. (3-4) still apply, but now the enthalpy and pressure are related by the same EOS on both sides of the interface. These equations give the temperature  $T_+$  as a function of the boundary value  $T_N$ , as well as the velocity of the shock front. The fluid is reheated in front of the wall, i.e.,  $T_+ > T_-$ ,  $T_N$ .

Notice that the velocity of a weak deflagration is in the range  $0 < v_w < c_{s-}$ . On the other hand, the velocity of a weak detonation is in the range  $v_J < v_w < 1$ , where  $v_J$  is the Jouguet detonation velocity, corresponding to the value of  $|v_+|$  at  $|v_-| = c_{s-}$  for the detonation curve. The latter is supersonic (see Fig. 2). The velocity gap between  $c_{s-}$  and  $v_J$  is filled by a family of supersonic Jouguet deflagrations. These solutions fulfil the Jouguet condition  $v_- = -c_{s-}$ , as well as the deflagration condition  $|v_+| < |v_-|$ , i.e., the fluid comes in subsonically, and goes out at the speed of sound. Nevertheless, the fluid on both sides moves forward with the wall, and the wall velocity with respect to the bubble center is not  $c_{s-}$ .



but higher. The velocity profile behind the wall is as in the case of the Jouguet detonation (right panel of Fig. 3). On the other hand, in front of the wall we have  $v_+ > v_-$ , and the profile shows a shock front discontinuity (for details, see, e.g., [11]).

It is important to stress that, for a given value of  $T_N$ , the Jouguet deflagrations are a whole set of solutions with velocities ranging from  $v_w = c_{s-}$  to  $v_w = v_J$  (both values depend on  $T_-$ , which, in turn, depends on  $T_N$ ). In contrast, the Jouguet detonation is a single solution, corresponding to the lowest possible value of the detonation velocity,  $v_w = v_J$ .

From the above, it is apparent that hydrodynamics alone does not determine the value of the wall velocity. An additional equation is needed, corresponding to the balance between the driving and friction forces.

### C. Equation for the interface

In order to obtain a macroscopic equation for the bubble wall, we need to consider the microphysics inside this thin interface, which is described by Eq. (2). Consider a reference frame at the center of the wall (thus, the field profile only varies in a small region around  $z = z_w = 0$ ). In the steady state, this frame moves at constant velocity, and only  $z$  derivatives appear in Eq. (2). We multiply by  $\phi' \equiv d\phi/dz$  and then we integrate across the wall (notice that  $\phi'$  vanishes outside the wall). Using the relation  $(\partial\mathcal{F}/\partial\phi)d\phi = d\mathcal{F} - (\partial\mathcal{F}/\partial T)dT$ , we obtain [17, 21]

$$\sigma \ddot{z}_w = F_{\text{dr}} + F_{\text{fr}}, \quad (17)$$

where  $\sigma$  is the surface tension,

$$\sigma \equiv \int \phi'^2 dz, \quad (18)$$

$F_{\text{dr}}$  is the force (per unit area) driving the propagation of the phase transition front,

$$F_{\text{dr}} = p_-(T_-) - p_+(T_+) + \int_{T_-}^{T_+} \frac{\partial\mathcal{F}}{\partial T} dT, \quad (19)$$

and  $F_{\text{fr}}$  is the friction force,

$$F_{\text{fr}} = \int \frac{\gamma v \tilde{\eta}(\phi')^2}{\sqrt{1 + (\gamma v)^2 \tilde{\lambda}^2(\phi')^2}} dz, \quad (20)$$

which depends explicitly on the velocity of the wall with respect to the fluid,  $-v$  (notice that  $F_{\text{fr}}$  is negative since we have  $v < 0$ ).

In order to obtain macroscopic expressions which do not depend on the wall shape, we will approximate the integrals in Eqs. (19) and (20). For the integral (20), we notice that the function  $\phi'(z)^2$  peaks inside the wall. Therefore, its presence in the numerator will select values of the integrand around  $z \approx 0$ . Hence, inside the square root in the denominator, we will just approximate  $\phi'^2$  by its value at the center of the wall,  $\phi_0'^2$ , whereas in the numerator, we will approximate it by a delta function  $\phi_0'^2 l_w \delta(z)$ , where  $l_w$  is the wall width. Furthermore, we may approximate the value of  $\phi_0'^2$  by  $(\Delta\phi/l_w)^2$ , where  $\Delta\phi$  is the field variation  $\phi_+ - \phi_-$ . The details of the approximations are not relevant, since all these parameters will be absorbed in the free parameters  $\tilde{\eta}$  and  $\tilde{\lambda}$ . Indeed, we define  $\eta = \tilde{\eta}(\Delta\phi)^2/l_w$ ,  $\lambda = \tilde{\lambda}\Delta\phi/l_w$ . With these approximations, the integrand now depends only

on  $v$ , which we assume has a smooth variation between  $v_-$  and  $v_+$ . We thus have an integral of the form  $\int f(z)\delta(z)dz = f(0)$ . Since we do not know the exact value of  $f(0)$ , we shall approximate it by the average of its values on each side of the wall,  $\langle f \rangle \equiv (f_+ + f_-)/2$ . We thus obtain [17]

$$F_{\text{fr}} = \left\langle \frac{\eta \gamma v}{\sqrt{1 + \lambda^2 (\gamma v)^2}} \right\rangle. \quad (21)$$

For a given model, the values of  $\eta$  and  $\lambda$  can be obtained by comparing the non-relativistic and ultra-relativistic limits of Eq. (21) with the corresponding results from microphysics calculations [17]. Indeed, notice that, for small  $v_w$ , we have  $F_{\text{fr}} = -\eta v_w$ , while for  $v_w \rightarrow 1$  we have  $F_{\text{fr}} = -(\eta/\lambda)v_w$ .

For the integral in Eq. (19), we may just use a linear approximation for the integrand inside the wall. It is useful to use, first, the identity  $(\partial \mathcal{F}/\partial T)dT = (\partial \mathcal{F}/\partial T^2)dT^2$  to obtain an expression in terms of  $T^2$ . This is convenient since  $\mathcal{F}$  is often quadratic. Thus, we obtain,

$$F_{\text{dr}} = p_-(T_-) - p_+(T_+) + \left\langle \frac{dp}{dT^2} \right\rangle (T_+^2 - T_-^2). \quad (22)$$

The second term in Eqs. (19) and (22) is due to hydrodynamic effects. This term is very important, since the driving force cannot be exclusively determined by the pressures outside the wall. For instance, for a deflagration, as we have seen, we have  $p_-(T_-) - p_+(T_+) < 0$ .

Since the friction force increases with the velocity, the wall may reach a terminal velocity, given by the equation  $F_{\text{fr}} = -F_{\text{dr}}$ . Such a stationary state will be reached in a time which is very short in comparison to the duration of a phase transition. Indeed, according to Eq. (17), the time scale associated to the acceleration of the wall is given by the quantity

$$d = \frac{\sigma}{F_{\text{dr}}}. \quad (23)$$

Since  $\sigma$  and  $F_{\text{dr}}$  are determined by the scale of the phase transition, this quantity is roughly given by  $d \sim 1/T$ , while the duration of the phase transition is roughly given by the cosmological time scale  $t \sim M_P/T^2$ , where  $M_P$  is the Plank mass. Notice that the ratio in Eq. (23) gives also a length scale associated to the balance between the driving force and the surface tension, in the case of a deformed wall (see the next section).

If a stationary state is reached, the terminal velocity is given by the equation

$$\eta \langle \gamma_\lambda v \rangle = -F_{\text{dr}}, \quad (24)$$

where we have rewritten the friction force (21) in terms of the quantity

$$\gamma_\lambda = \frac{1}{\sqrt{1 - (1 - \lambda^2)v^2}}. \quad (25)$$

This equation can be solved using Eqs. (3-4) and appropriate boundary conditions.

#### D. Runaway walls

In the particular case  $\lambda = 0$ , we have  $\gamma_\lambda = \gamma$ , and the friction force grows as  $\gamma v$ . In such a case, the wall will always reach a terminal velocity  $v_w < 1$ . On the other hand, for

nonvanishing  $\lambda$ , the friction saturates at the value  $F_{\text{fr}} = -\eta/\lambda$  in the ultra-relativistic limit. If the driving force (which depends on the amount of supercooling and on hydrodynamics) is larger than this value, a terminal velocity will not be reached, i.e., the wall will run away. The condition for non-existence of stationary solutions is thus

$$F_{\text{dr}} > \eta/\lambda, \quad (26)$$

with  $F_{\text{dr}}$  given by Eq. (22). Notice that the condition (26) can be reached only in the ultra-relativistic limit. Therefore, as a function of the parameters, Eq. (26) is a condition for the nonexistence of *detonations*. Indeed, for a given set of parameters, the detonation solution may fulfill Eq. (26) (which means that its velocity would exceed the speed of light), but it may happen that we still have a deflagration solution, for which the driving force is much smaller (due to different hydrodynamics). Hence, deflagrations may coexist with runaway solutions, even when detonations do not.

Detonations may also coexist with runaway solutions. Indeed, a runaway solution may exist even if Eq. (26) is not fulfilled. This is possible because, for extremely high values of  $\gamma v$ , the hydrodynamics is different and  $F_{\text{dr}}$  is not given by Eq. (22) anymore [15, 17]. In this case, the particles distribution functions are essentially unaffected as they pass through the wall. The *total* force in this limit is given by the difference  $F_{\text{tot}} = \mathcal{F}_+(T_+) - \tilde{\mathcal{F}}_-(T_+)$ , where  $\tilde{\mathcal{F}}_-(T_+)$  is the mean field effective potential, obtained by keeping only the quadratic terms in a Taylor expansion about the  $+$  phase [10, 15]. In our phenomenological model, this total force is given by  $F_{\text{tot}} = p_-(T_+) - p_+(T_+) - \eta/\lambda$  (see [17] for details). Therefore, the condition for the existence of a runaway solution is

$$p_-(T_+) - p_+(T_+) > \eta/\lambda. \quad (27)$$

For given values of the friction parameters, both conditions (26) and (27) will be fulfilled for high enough supercooling (i.e., small enough values of  $T_+/T_c$ ). Nevertheless, it is important to notice that, when the condition (27) is already fulfilled, the condition (26) may not be fulfilled yet. Indeed, for a stationary solution the driving force is smaller than  $p_-(T_+) - p_+(T_+)$  (due to hydrodynamic effects). Hence, even if the runaway solution exists, the wall may still not run away, since a detonation solution may exist as well. In the case of coexistence of a stationary solution and a runaway solution, one expects that the former will be the one to be realized in the phase transition, unless it is unstable.

### E. A specific example: the bag EOS

The simplest phenomenological equation of state for a phase transition is the well known bag EOS, which consists of radiation and vacuum energy. The pressure in each phase can be written in the form

$$p_+(T) = \frac{a}{3}T^4 - \frac{L}{4}, \quad p_-(T) = \left( \frac{a}{3} - \frac{L}{4T_c^4} \right) T^4. \quad (28)$$

The thermodynamic quantities can be obtained from  $s = dp/dT$ ,  $w = Ts$ ,  $e = Ts - p$ . This model has three free parameters, namely, the critical temperature  $T_c$ , the latent heat  $L$ , and the coefficient  $a$ . The latter is related to the number of degrees of freedom of radiation in the  $+$  phase. The speed of sound is the same in both phases,  $c_s = 1/\sqrt{3}$ .

In this model, the driving force (22) takes the form

$$F_{\text{dr}} = \frac{L}{4} \left( 1 - \frac{T_-^2 T_+^2}{T_c^4} \right). \quad (29)$$

The matching conditions (3-4) give the relations

$$\frac{T_-^2}{T_+^2} = \sqrt{\frac{v_+ \gamma_+^2}{v_- \gamma_-^2 (1 - \bar{L})}}, \quad (30)$$

$$v_- = \frac{1}{6v_+} \left[ 1 - 3\alpha + 3(1 + \alpha) v_+^2 \pm \sqrt{[1 - 3\alpha + 3(1 + \alpha) v_+^2]^2 - 12v_+^2} \right], \quad (31)$$

where

$$\bar{L} \equiv \frac{L}{4aT_c^4/3} = \frac{L}{w_+(T_c)}, \quad (32)$$

and

$$\alpha \equiv \frac{L}{4aT_+^4} = \frac{\bar{L}}{3} \frac{T_c^4}{T_+^4}. \quad (33)$$

The + sign in Eq. (31) corresponds to weak detonations or strong deflagrations (i.e.,  $|v_-| > c_s$ ), while the − sign corresponds to strong detonations or weak deflagrations ( $|v_-| < c_s$ ). At the Jouguet point, we have  $v_- = -c_s$  and

$$v_+ = -v_J \equiv -\frac{1/\sqrt{3} \pm \sqrt{\alpha^2 + 2\alpha/3}}{1 + \alpha}. \quad (34)$$

Here, the + and − signs correspond to detonations and deflagrations, respectively.

Using the above relations, we can obtain the stationary wall velocity from Eq. (24). For deflagrations, the boundary conditions give  $v_w = -v_-$ . Besides, the temperature  $T_+$  is obtained by applying Eqs. (3-4) to the shock front discontinuity. This gives

$$\frac{\sqrt{3} (T_+^4 - T_N^4)}{\sqrt{(3T_+^4 + T_N^4)(3T_N^4 + T_+^4)}} = \frac{v_+ - v_-}{1 - v_+ v_-}. \quad (35)$$

For detonations, in contrast, the fluid is not reheated in front of the wall, and we have simpler conditions, namely,  $T_+ = T_N$ ,  $v_w = -v_+$ .

The condition (27) for existence of runaway solutions gives, for the bag EOS,

$$1 - \frac{T_N^4}{T_c^4} > \frac{4}{\lambda} \frac{\eta}{L}. \quad (36)$$

On the other hand, according to Eq. (26), detonations cannot exist if

$$1 - \frac{T_-^2 T_N^2}{T_c^4} > \frac{4}{\lambda} \frac{\eta}{L}. \quad (37)$$

For a complete description of the solutions, see Ref. [17]. Here, we are primarily interested in weak detonations. In Fig. 4 we show the weak detonation velocity as a function of the friction parameter  $\eta$  (solid lines). We considered two different amounts of supercooling (left

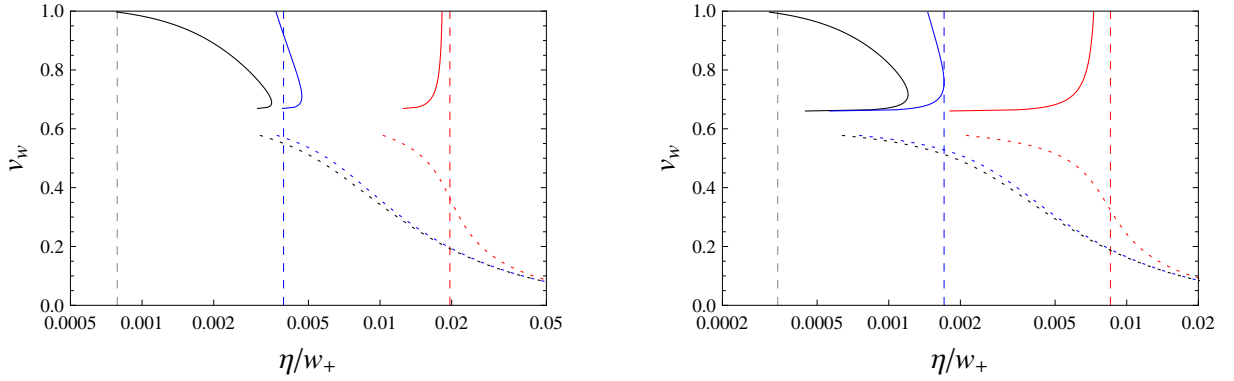


FIG. 4: The wall velocity as a function of the friction parameter  $\eta$ , for  $\lambda = 0.2$  (black),  $\lambda = 1$  (blue), and  $\lambda = 5$  (red). Solid lines correspond to weak detonations and dotted lines to weak deflagrations. The vertical dashed lines indicate the values of  $\eta$  below which runaway is possible for each value of  $\lambda$ . The latent heat parameter is given by  $\bar{L} = 0.03$ , and the amount of supercooling is  $T_N/T_c = 0.9$  (left panel), and  $T_N/T_c = 0.95$  (right panel).

and right panels), both of which are strong enough (for the given value of the latent heat) for the existence of detonations and runaway solutions. For comparison, we show also the weak deflagration solutions (dotted lines). We considered a few values of  $\lambda$  which give different behaviors of the friction force, namely,  $\lambda = 0.2$  (in black),  $\lambda = 1$  (in blue), and  $\lambda = 5$  (in red).

It is apparent that the value of  $\lambda$  affects especially supersonic velocities. The value  $\lambda = 1$  is not special, but is representative for the case in which the “friction coefficient”  $|F_{\text{fr}}/v_w|$  has similar values in the non-relativistic and ultra-relativistic limits. The value  $\lambda = 0.2$  corresponds to a high ultra-relativistic friction, while the value  $\lambda = 5$  corresponds to a small ultra-relativistic friction. Except in the limit  $\lambda \rightarrow 0$ , the friction saturates at high velocities and the detonation approaches the speed of light at a finite value of  $\eta$ , which is given by Eq. (37). Below this value, we have no detonations, and the wall runs away. The existence of the runaway solution, on the other hand, is determined by Eq. (36). The value of  $\eta$  below which runaway is already possible is indicated in Fig. 4 by the vertical dashed lines.

For large values of  $\eta$ , the wall velocity is small and the hydrodynamic process is a deflagration. As  $\eta$  is decreased, the velocity increases. However, the velocity does not grow as  $v_w \sim 1/\eta$ , as Eq. (24) may suggest, since hydrodynamic effects act as an effective friction [9, 12]. Indeed, the reheating of the plasma slows down the wall, since the driving force (29) decreases as any of the temperatures  $T_{\pm}$  approaches  $T_c$ .

Below a certain value  $\eta = \eta_{\text{max}}$ , we have detonations in addition to deflagrations. Notice that we have in general two weak detonation solutions. One of them behaves “normally” with  $\eta$ , i.e., the velocity increases as the friction decreases. This branch of solutions ends with a velocity  $v_w = 1$ . The other branch corresponds to stronger weak detonations and ends at the Jouguet point. This branch behaves rather unphysically, since the velocity decreases as the friction decreases. This means that the fluid disturbances cause a strong friction effect. Indeed, the reheating is significant near the Jouguet point. This can be appreciated in Fig. 5, where we show the reheating as a function of  $v_w$  for the two values of  $T_N$  considered in Fig. 4. Notice that, for  $v_w \simeq 1$ , the temperature  $T_-$  is quite close to  $T_N$ . However, as the

velocity decreases, the reheating increases, and we may even have  $T_- > T_c$  as the Jouguet velocity is approached.

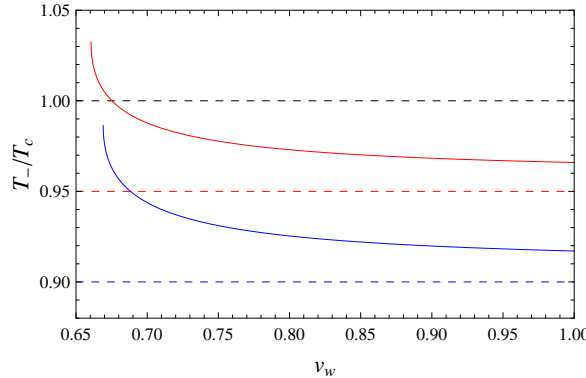


FIG. 5: The fluid temperature  $T_-$  (solid lines) as a function of the detonation wall velocity, for  $\bar{L} = 0.03$ , and for  $T_N/T_c = 0.9$  (in blue) and  $T_N/T_c = 0.95$  (in red). Dashed lines indicate the values of  $T_N$  as well as the critical temperature.

It is worth commenting that the deflagration solutions have a similar behavior, i.e., if the deflagration curve in Fig. 4 is continued beyond the speed of sound, it becomes double-valued (see, e.g., [13]). However, this occurs for strong deflagrations, which are unstable [21]. In the case of detonations, in contrast, this behavior occurs already for weak solutions, although the “unphysical” branch is closer to the Jouguet point and, thus, corresponds to stronger weak detonations.

### F. Physical and unphysical weak detonations

The example considered in the previous subsection (the bag EOS) shows an interesting feature of weak detonations, namely, the existence, in a certain range of parameters, of two solutions. Although the lower velocity branch has a strange dependence on the parameters, these solutions are not physically forbidden. Their behavior is due to strong hydrodynamics effects. We shall now analyze this feature in detail, without specifying any equation of state.

Let us consider the dependence of  $v_w$  on the friction and the amount of supercooling. Differentiating Eq. (24), we have

$$-\langle v\gamma_\lambda \rangle d\eta + \eta \langle v^3 \gamma_\lambda^3 \rangle \lambda d\lambda - \frac{\partial F_{\text{dr}}}{\partial T_+} dT_N = Q dv_w, \quad (38)$$

with

$$Q = -\frac{\eta}{2} \left( \gamma_{\lambda w}^3 + \gamma_{\lambda-}^3 \frac{\partial v_-}{\partial v_+} \right) + \frac{\partial F_{\text{dr}}}{\partial T_-} \frac{T_-}{w_-} \frac{c_{s-}^2}{1 + c_{s-}^2} \frac{\partial w_-}{\partial v_w}, \quad (39)$$

where  $\partial v_- / \partial v_+$  and  $\partial w_- / \partial v_w$  are given by Eqs. (9-10). Therefore, the derivatives of  $v_w$  with respect to any of the parameters  $\eta$ ,  $\lambda$ , or  $T_N$  are inversely proportional to the factor  $Q$ , and share some essential properties. Consider, for instance,  $T_N$  and  $\lambda$  fixed. We have

$$\partial \eta / \partial v_w = Q / \langle -v\gamma_\lambda \rangle. \quad (40)$$

Since  $-v$  is positive, the sign of  $\partial\eta/\partial v_w$  depends on the two terms in Eq. (39). The first term is negative, since  $\partial v_-/\partial v_+$  is positive for weak detonations. On the other hand, the second term is positive, since we have  $\partial F_{\text{dr}}/\partial T_- < 0$  (the driving force increases as  $T_{\pm}$  decrease) and  $\partial w_-/\partial v_w < 0$ , as can be seen in Eq. (10) (for weak detonations). The first term in Eq. (39) is due to the dependence of the friction force on the velocity. This term would give a “normal” variation of  $v_w$  with  $\eta$  (i.e.,  $v_w$  decreasing with  $\eta$ ). On the other hand, the second term comes from  $\partial F_{\text{dr}}/\partial v_w$  and is due entirely to hydrodynamics. Indeed, notice that the driving force does not depend on the wall velocity explicitly, but only through the temperature  $T_-$ .

The negative sign of  $\partial w_-/\partial v_w$  implies that, the higher the velocity, the smaller the reheating behind the wall. This means that the hydrodynamics is always weaker for higher velocities. The strengthening of hydrodynamics effects as the Jouguet point is approached is apparent in Eqs. (9-10) if we notice the dependence on the two parameters  $v_+ - v_-$  and  $v_-^2 - c_-^2$ . The former is the velocity discontinuity across the interface, which vanishes for  $v_w \rightarrow 1$  and is maximum at the Jouguet point (see Fig. 2). In Eqs. (9-10), this maximum is further emphasized by the divergence due to the factor  $v_-^2 - c_-^2$  in the denominators. Thus, for very weak detonations (i.e., in the limit  $v_w \rightarrow 1$ ), we have a finite value of  $\partial v_-/\partial v_+$  (namely,  $\partial v_-/\partial v_+ = \gamma_+^2/\gamma_-^2 = w_-/w_+$ ), and a vanishing  $\partial w_-/\partial v_w$ , (hence, a variation of the wall velocity does not alter the reheating temperature). On the other hand, at the Jouguet point both  $\partial v_-/\partial v_+$  and  $\partial w_-/\partial v_w$  diverge. These are the behaviors observed for the particular cases considered in Figs. 2 and 5.

Obtaining the effect of this hydrodynamics on the wall velocity is straightforward from Eq. (40). For  $v_w$  close to 1, we will have  $\partial v_w/\partial \eta < 0$ , since the second term in Eq. (39) will be vanishingly small. On the other hand, at the Jouguet point we will have  $\partial v_w/\partial \eta = 0$ , since both terms of  $Q$  diverge (cf. Fig. 4 for the particular case of the bag EOS). Besides, near the Jouguet point, we will see that the second term in (39) becomes larger than the first one. Hence, we have  $\partial v_w/\partial \eta > 0$ , i.e., we obtain the “unphysical branch” of weak detonations. Indeed, replacing in Eq. (39) the expressions for  $\partial v_-/\partial v_+$  and  $\partial w_-/\partial v_w$  given by Eqs. (9-10), it can be seen that  $Q$  vanishes at a velocity  $v_{\text{crit}}$  given by the equation

$$\gamma_-^{-1} \left\langle \frac{\gamma_\lambda^3}{\gamma^2} \right\rangle \frac{v_-^2 - c_{s-}^2}{c_{s-}^2} = \left( \beta_- - \frac{v_-^2 + c_{s-}^2}{2c_{s-}^2} \frac{\gamma_{\lambda-}^3}{\gamma_-^3} \right) \frac{1 - v_+ v_-}{1 - v_-^2} \frac{\Delta v}{v_+}, \quad (41)$$

where

$$\beta_- = \frac{\langle \gamma_\lambda v \rangle v_-}{\gamma_-} \frac{2T_-}{F_{\text{dr}}} \left( -\frac{\partial F_{\text{dr}}}{\partial T_-} \right). \quad (42)$$

The velocity  $v_{\text{crit}}$  corresponds to the maximum  $\eta_{\text{max}}$  of the curve of  $\eta$  vs  $v_w$ . Provided that the factor in parenthesis in Eq. (41) is positive, the equation will be satisfied for a velocity  $v_{\text{crit}}$  between the Jouguet value  $v_J$  and the speed of light. We shall see that this is indeed the case. Hence, the curve of  $v_w$  vs  $\eta$  is always of the form of Fig. 4.

To see that the factor in parenthesis in Eq. (41) is in general positive, notice that the second term inside the parenthesis is at most  $\sim 1$  for  $|v_-|$  between  $c_{s-}$  and 1. On the other hand, in  $\beta_-$  we distinguish two factors of different nature<sup>6</sup>. The first factor depends on the

---

<sup>6</sup> The parameter  $\beta_-$  is associated to the fluid perturbations behind the wall, and will appear again when we consider the stability of the stationary solution in the next section.

velocity and is  $\sim v_w^2$ , whereas the second factor contains the information on the equation of state. We may write

$$\beta_- \sim v_w^2/v_c^2, \quad (43)$$

with

$$v_c^2 \propto \frac{F_{\text{dr}}}{T_- \partial F_{\text{dr}} / \partial T_-}. \quad (44)$$

For weak detonations,  $v_w$  is supersonic, while the velocity parameter  $v_c$  is in general very small. Indeed,  $v_c^2$  gives a dimensionless measure of the driving force, which is very small for  $T_{\pm}$  close to  $T_c$ . Hence, we will generally have  $\beta_- \gg 1$ . In particular, the large reheating near the Jouguet point will cause a very small  $F_{\text{dr}}$ . Physically, this effect prevents the velocity to increase as the friction decreases, and causes the lower velocity branch of weak detonations.

For the sake of concreteness, let us consider again the bag EOS, for which we have

$$\beta_- = \frac{\gamma_-^{-1} \langle \gamma_{\lambda} v \rangle v_-}{\frac{1}{4} \left( \frac{T_c^4}{T_-^2 T_+^2} - 1 \right)} \quad (\text{bag}). \quad (45)$$

For small reheating ( $T_- \simeq T_+ = T_N$ ), the denominator is given by  $\frac{1}{4} (T_c^4/T_N^4 - 1)$ . Consider for instance the electroweak phase transition. For different extensions of the Standard Model, the value of  $T_N/T_c$  is typically in the range  $0.8 - 1$ , while very strong phase transitions may reach a supercooling of  $T_N/T_c \simeq 0.7$  [21]. For this lower limit, we have  $\frac{1}{4} (T_c^4/T_N^4 - 1) \simeq 0.8$ . However, a large supercooling will be accompanied in general by a large latent heat, since both are characteristics of a strong phase transition. Even disregarding the reheating caused by the release of latent heat, for such a large supercooling we expect a high velocity,  $v_w > 0.9$ , and the numerator in (45) will be  $\sim v_w^2 > 0.8$ . Therefore, even in such an extreme case, we expect  $\beta_- \gtrsim 1$ . Due to reheating, the denominator in Eq. (45) will be in general quite smaller than  $\frac{1}{4} (T_c^4/T_N^4 - 1)$ . As we have seen, we may even have  $T_- > T_c$ . Thus, in the general case we will have  $\beta_- \gg 1$ .

### III. STABILITY ANALYSIS OF WEAK DETONATIONS

The structure of multiple stationary solutions observed in Fig. 4 was found in different numerical calculations (see e.g. [24]). There exist also supersonic Jouguet deflagrations (not shown in Fig. 4 for simplicity), which also coexist with detonations in some parameter ranges. Besides, as we have seen, there are ranges of coexistence with runaway walls. The coexistence of hydrodynamic solutions is an important issue, since one has to determine which of these will be realized during the phase transition. Investigating the stability of the stationary motion may help deciding which solutions to choose. In particular, one expects that the “unphysical” weak detonations described above should not be realized [9]. As a matter of fact, numerical simulations suggest that the detonations which are closer to the Jouguet point are unstable [24]. We shall now consider the linear stability of the weak detonation solution.

#### A. Linear perturbations

We shall consider small variations of the wall position  $\zeta(x^{\perp}, t)$  around a planar interface. For planar symmetry, we only need to consider a single direction  $x^{\perp}$  transverse to the wall



motion. Besides, we need to consider, on each side of the wall, the longitudinal perturbation of the velocity  $\delta v(x^\perp, z, t)$  and the transverse velocity  $v^\perp(x^\perp, z, t)$ , as well as the pressure fluctuation  $\delta p(x^\perp, z, t)$  (the latter may be replaced by the temperature fluctuation  $\delta T$ ).

The standard approach (see, e.g., [20–23]) consists in considering small perturbations around a solution with  $v = \text{const}$  and  $T = \text{const}$ . This allows to consider Fourier modes and, hence, to deal with algebraic equations (dispersion relations). It is worth remarking that this assumption is not always valid. Such is the case, for instance, of the fluid profile for the Jouguet detonation (Fig. 3, right panel). Perturbing this profile gives much more involved equations and is out of the scope of this work.

For the weak detonation solution depicted in the left panel of Fig. 3, the fluid profile is a constant in front of the wall. Behind the wall, the profile is a constant up to a point  $z_0 = \xi_0 t$ , with  $\xi_0$  given by Eq. (15). Beyond this point, we have the rarefaction wave  $v_{\text{rar}}(z/t)$ . In general, assuming a constant profile is a good approximation for perturbations originated at the wall. Indeed, the Fourier modes will decay as  $e^{-q|z|}$  away from the wall, within a distance scale  $q^{-1}$  which will be given, in general, by  $q^{-1} \sim d$ . In contrast, the zone of constant  $v$  and  $T$  will grow quickly to values  $|\xi_0 t| \gg d$ , since the scale  $d$  is much smaller than the time associated to bubble expansion [see the discussion below Eq. (23)]. This approach will break down, anyway, for weak detonations which are very close to the Jouguet point, where  $\xi_0$  vanishes.

### 1. Fluid equations and junction conditions

The equations for the fluid perturbations have been considered recently in Ref. [21], and we shall only write down the results. We shall consider a reference frame moving with the unperturbed wall. The equations for the fluid perturbations, as well as their matching conditions at the interface, are derived by considering Eqs. (1) as in the previous section, this time for the perturbed variables, and keeping to linear order in the perturbations. For the fluid away from the wall, we have

$$c_s^2 w (\gamma^2 v \delta v_{,0} + \gamma^2 \delta v_{,z} + v_{,\perp}^\perp) + \delta p_{,0} + v \delta p_{,z} = 0, \quad (46)$$

$$w \gamma^2 (\delta v_{,0} + v \delta v_{,z}) + v \delta p_{,0} + \delta p_{,z} = 0, \quad (47)$$

$$w \gamma^2 (v_{,0}^\perp + v v_{,z}^\perp) + \delta p_{,\perp} = 0, \quad (48)$$

while the matching conditions at the interface are given by

$$\Delta [w \gamma^2 (1 + v^2) (-\partial_0 \zeta + \gamma^2 \delta v) + (1 + c_s^{-2}) \gamma^2 v \delta p] = 0, \quad (49)$$

$$\Delta (v^\perp + v \partial_\perp \zeta) = 0, \quad (50)$$

$$\sigma (\partial_0^2 - \partial_\perp^2) \zeta + \Delta [2w \gamma^4 v \delta v + (1 + (1 + c_s^{-2}) \gamma^2 v^2) \delta p] = 0, \quad (51)$$

where  $\Delta$  applied to any function  $f$  means  $f_+ - f_-$ . Notice that these equations depend on the equation of state only through the parameter  $c_s$ .

### 2. Equation for the interface

The equation for the interface perturbations is obtained from the field equation (2), like in the previous section. We have already derived this equation in Ref. [21]. However,

we considered a simplified version of the damping term in Eq. (2), corresponding to the particular case  $\lambda = 0$ . As can be seen in Fig. 4, this is generally a good approximation for deflagrations but not for detonations, which depend strongly on  $\lambda$ . We shall consider here the general case.

We consider perturbations around a stationary wall, which is at  $z_w = 0$ , and for which we have  $\dot{z}_w = \ddot{z}_w = 0$ . On the other hand, the perturbed wall is at the position  $z_w = \zeta(x^\perp, t)$ . We thus assume a field profile<sup>7</sup> of the form  $\phi(z, x^\perp, t) = \phi[z - \zeta(x^\perp, t)]$ . To first order in  $\zeta$  and  $v^\perp$ , we have  $\partial_\mu \partial^\mu \phi = \phi'(\partial_\perp^2 - \partial_0^2)\zeta - \phi''$  and  $u^\mu \partial_\mu \phi = \gamma(-\partial_0 \zeta + v)\phi'$ . Multiplying Eq. (2) by  $\phi'(z - \zeta)$  and integrating in  $z$ , we obtain

$$\sigma(\partial_0^2 - \partial_\perp^2)\zeta = F_{\text{dr}}[T] + F_{\text{fr}}[\gamma(v - \partial_0 \zeta)], \quad (52)$$

where the forces  $F_{\text{dr}}[T]$ ,  $F_{\text{fr}}[\gamma v]$  are given by Eqs. (19) and (20) as functionals of the temperature and velocity configurations. We notice the following differences with Eq. (17). The term  $-\sigma \partial_\perp^2 \zeta$  gives the restoring force due to the curvature of the surface. The argument of the driving force is now the perturbed temperature,  $T \rightarrow T + \delta T$ . The velocity  $v$  in the friction force is the perturbed one,  $v \rightarrow v + \delta v$ , and the argument of  $F_{\text{fr}}$  is further modified by the term  $-\partial_0 \zeta$ . To understand this dependence, notice that the friction must depend on the *relative* velocity  $v_r$  between the fluid and the wall, which is given by the relation  $\gamma_r v_r = \gamma(v - \partial_0 \zeta)$ .

We may use the approximations for the force functionals derived in Sec. II in terms of the values of the variables outside the wall,

$$F_{\text{dr}}[T] \simeq F_{\text{dr}}(T_+, T_-), \quad F_{\text{fr}}[\gamma v] \simeq F_{\text{fr}}(\gamma_+ v_+, \gamma_- v_-), \quad (53)$$

where we must do the replacements  $T \rightarrow T + \delta T$ ,  $\gamma v \rightarrow \gamma v + \delta(\gamma_r v_r)$  in each argument. Hence, the perturbations from the stationary case are given by

$$\delta F_{\text{dr}} = \frac{\partial F_{\text{dr}}}{\partial T_+} \delta T_+ + \frac{\partial F_{\text{dr}}}{\partial T_-} \delta T_-, \quad (54)$$

$$\delta F_{\text{fr}} = \frac{\partial F_{\text{fr}}}{\partial(\gamma_+ v_+)} [\delta(\gamma_+ v_+) - \gamma_+ \partial_0 \zeta] + \frac{\partial F_{\text{fr}}}{\partial(\gamma_- v_-)} [\delta(\gamma_- v_-) - \gamma_- \partial_0 \zeta]. \quad (55)$$

Using Eq. (21), Eq. (52) gives

$$\sigma(\partial_0^2 - \partial_\perp^2)\zeta = 2 \left\langle \frac{\partial F_{\text{dr}}}{\partial T} \delta T \right\rangle + \eta \left\langle \frac{\delta(\gamma v) - \gamma \partial_0 \zeta}{(1 + \lambda^2 \gamma^2 v^2)^{3/2}} \right\rangle. \quad (56)$$

The parameters  $\sigma$  and  $\eta$  can be written in terms of the fluid velocity and the scale  $d$  using Eqs. (24) and (23). Furthermore, the temperature variation is related to our perturbation variable  $\delta p$  through  $\delta p = s \delta T$ . Thus, we may write

$$\left\langle \gamma_\lambda v d (\partial_0^2 - \partial_\perp^2) \zeta + \gamma_\lambda^3 \delta v - \frac{\gamma_\lambda^3}{\gamma^2} \partial_0 \zeta + \frac{\gamma \beta}{v} \frac{\delta p}{w} \right\rangle = 0, \quad (57)$$

where the parameters  $\beta_\pm$  contain information about the equation of state (we have already introduced  $\beta_-$  in the previous section),

$$\beta_\pm = \frac{\langle \gamma_\lambda v \rangle v_\pm}{\gamma_\pm} \frac{2T_\pm}{F_{\text{dr}}} \left( -\frac{\partial F_{\text{dr}}}{\partial T_\pm} \right) = \frac{\langle \gamma_\lambda v \rangle v_\pm}{\gamma_\pm} \frac{4T_\pm^2}{F_{\text{dr}}} \left( -\frac{\partial F_{\text{dr}}}{\partial T_\pm^2} \right). \quad (58)$$

The last equality is useful if  $F_{\text{dr}}$  is quadratic in the temperature [21].

---

<sup>7</sup> The small perturbation  $\zeta$  is macroscopic in comparison with the wall width  $l_w$ .

### B. Fourier modes of the perturbations

The fluid equations away from the wall, Eqs. (46-48), can be expressed in matrix form, defining the perturbation vector

$$\vec{U} \equiv \begin{bmatrix} \delta p \\ \delta v \\ v^\perp \end{bmatrix}. \quad (59)$$

We are interested in solutions of the form

$$\vec{U}(t, z, x^\perp) = \vec{L} e^{\Omega t + qz + ikx^\perp}, \quad (60)$$

where  $k$  is a real wavenumber corresponding to Fourier modes along the wall, and  $\Omega, q$  are in general complex numbers. The stationary solution will be unstable if there are modes with  $\text{Re}(\Omega) > 0$ . Inserting Eqs. (59-60) into the fluid equations we obtain an eigenvalue equation for the perturbation modes (for details, see [21]). This gives the dispersion relations

$$q_1 = -\Omega/v, \quad (61)$$

$$q_{2,3} = \frac{(1 - c_s^2)v\Omega \pm c_s(1 - v^2)\sqrt{\Omega^2 + (c_s^2 - v^2)\gamma^2 k^2}}{c_s^2 - v^2}, \quad (62)$$

corresponding to the eigenvectors

$$\vec{L}_1 = \begin{bmatrix} 0 \\ 1 \\ \frac{iq_1}{k} \end{bmatrix}, \quad \vec{L}_{2,3} = \begin{bmatrix} -w\gamma^2 \left( \frac{\Omega + q_{2,3}v}{\Omega v + q_{2,3}} \right) \\ 1 \\ \frac{ik}{\Omega v + q_{2,3}} \end{bmatrix} \quad (63)$$

The eigenvector  $\vec{L}_1$  is a special mode corresponding to a perturbation with  $\delta p = 0$ , which moves with the fluid (i.e., the perturbation is a function of  $z - vt$ ).

In Fig. 6 we show the real part of  $q$  as a function of the real part of  $\Omega$  for the three modes. For the special mode we have a linear relation between  $q$  and  $\Omega$ ,  $q_1 = \Omega/|v|$ . Regarding the solutions  $q_{2,3}$ , the relation is linear for  $k = 0$ ,

$$q_{2,3} = \Omega/a_{2,3}, \quad (64)$$

with

$$a_{2,3} = \frac{|v| \pm c_s}{1 \pm c_s|v|}. \quad (65)$$

For  $k \neq 0$ , the lines (64) are asymptotes for the curves of  $\text{Re}(q)$  vs.  $\text{Re}(\Omega)$ . These asymptotes depend on the value of  $v$ . We are interested in the weak detonation case, for which both  $v_+$  and  $v_-$  are supersonic (left panel of Fig. 6). In this case,  $\text{Re}(q)$  and  $\text{Re}(\Omega)$  have always the same sign. Notice that, in the limit  $|v| = c_s$ , one of the asymptotes becomes vertical and we are left with only two modes (central panel); specifically, we have  $q_1 = -\Omega/v$  and

$$q_2 = \frac{c_s k^2}{2\Omega} + \frac{(1 + c_s^2)}{2c_s} \Omega. \quad (66)$$

The subsonic case (right panel) is only relevant for deflagrations or strong detonations.

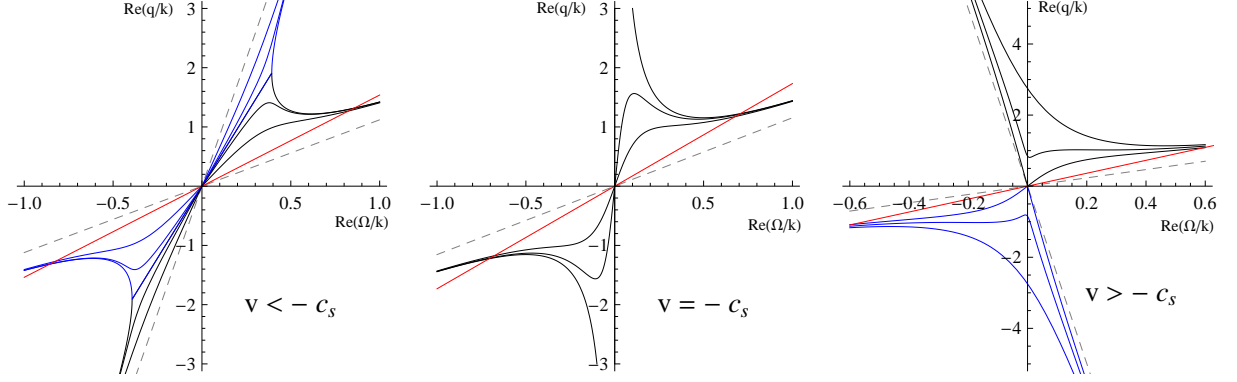


FIG. 6: The real parts of the dispersion relations  $q_1(\Omega)$  (in red),  $q_2(\Omega)$  (in black), and  $q_3(\Omega)$  (in blue), for different values of the imaginary part  $\text{Im}(\Omega)$ . Gray dashed lines indicate the asymptotes of these solutions.

For given  $k$  and  $\Omega$ , the general solution will be a superposition of these modes,

$$\vec{U}(t, z, x^\perp) = \vec{A}(z)e^{(\Omega t + i k x^\perp)}, \quad (67)$$

with

$$\vec{A}(z) = \sum_{j=1}^3 A_j \vec{L}_j e^{q_j z}, \quad (68)$$

where the constants  $A_j$  are different on each side of the wall. The function  $\vec{A}(z)$  must satisfy the junction conditions at the wall. On the other hand, the surface perturbation will be of the form

$$\zeta(t, x^\perp) = D e^{(\Omega t + i k x^\perp)}. \quad (69)$$

Notice that, for weak detonations, we always have  $\text{Re}(q) = 0$  for  $\text{Re}(\Omega) = 0$ . This case corresponds to undamped oscillations of the wall which generate plane waves in the fluid. Since we are looking for instabilities, we are interested in the case  $\text{Re}(\Omega) > 0$ . In this case, we have always  $\text{Re}(q) > 0$ . The condition that the source of instabilities is the wall itself, and not something outside it, implies that the perturbations must decrease with the distance from the wall [22]. Therefore, we must require  $\text{Re}(q) < 0$  for  $z > 0$  (i.e., in the  $+$  phase) and  $\text{Re}(q) > 0$  for  $z < 0$  (i.e., in the  $-$  phase).

The requirement  $\text{Re}(q) < 0$  in front of the wall implies, for detonations,  $\text{Re}(\Omega) < 0$ . This means that perturbations of the fluid in front of the wall decay exponentially. This is a consequence of the fact that the fluid enters the wall supersonically. The absence of unstable modes in the  $+$  phase led the authors of Ref. [20] to the conclusion that detonations are always stable. However, as pointed out in Ref. [25], perturbations in the  $-$  phase should also be considered. Behind the wall we require  $\text{Re}(q) > 0$ , for which we have  $\text{Re}(\Omega) > 0$  in the weak detonation case. Such a perturbation will grow exponentially. Thus, weak detonations may be unstable. Nevertheless, not any fluid perturbation will fulfill the junction conditions. We have just seen that perturbations which are localized near the wall have a different time dependence in front and behind the wall. Such perturbations cannot be matched. Therefore, if we look for unstable perturbations, we must consider a solution which is of the general form (68) behind the wall and *vanishes* in front it.

The approach of previous works [25, 26] to the stability of detonation fronts in a cosmological phase transition consisted essentially in solving the aforementioned matching conditions. However, the general treatment of these works is more suitable for chemical burning than for a phase transition. Although the case of chemical burning is out of the scope of the present paper, we wish to point out that, even in that case, some aspects of the treatment of Refs. [25, 26] seem to be incorrect.

In the first place, only strong and Jouguet detonations were considered in Refs. [25, 26]. We remark that, for a phase transition front, strong detonations are impossible, since the stationary profile cannot satisfy the boundary and junction conditions (see, e.g., [18, 19]). Therefore, this solution should not be considered from the beginning. In the case of chemical burning, according to the Chapman-Jouguet theory, strong detonations should decay to a Jouguet detonation.

In contrast, in the case of chemical burning, weak detonations are not possible. According to an argument by Steinhardt [18], this would also be the case of a cosmological phase transition. However, as already pointed out by Landau [22], a phase transition front must be treated differently than a burning front. In Ref. [19] it was shown, in particular, that weak detonations are possible in a cosmological phase transition.

In this regard, we may note, for instance, that in the case of chemical burning, the reheating of the fluid favors the combustion and, thus, the propagation of the burning front. In contrast, in the case of a phase transition, the reheating causes a decrease of the pressure difference between phases and, thus, opposes to the propagation of the front.

This last feature is taken into account by the interface equation, either Eq. (24) for the stationary case or Eq. (57) for the perturbed wall. No equation for the interface was considered in Refs. [25, 26]. Therefore, only the three junction conditions (49-51) were imposed on the system. In the case of Jouguet or strong detonations, this is compatible with the number of unknowns. Indeed, notice that, in the Jouguet case (central panel of Fig. 6), we have only two unstable modes in the  $-$  phase. Similarly, it can be seen from the right panel of Fig. 6 that, for strong detonations, we also have only two unstable modes. We thus have three unknowns, namely, the coefficients  $A_1$  and  $A_2$  of these modes, plus the coefficient  $D$  of the surface perturbation. By solving this system of equations, it was found in Ref. [25] that unstable modes exist at all wavelengths. In contrast with this result, in Ref. [26] it was found, with a similar treatment, that strong detonations can be stable and that Jouguet detonations are unconditionally stable.

In any case, an important feature seems to have been missed by the authors of Refs. [25] and [26], namely, that the usual approach of considering perturbations around a constant solution will break down for the profile of a Jouguet detonation, as already discussed.

Let us go back to the phase transition case. Notice that, if we take into account the surface equation (57) together with the junction conditions (49-51), then we have, for the Jouguet and the strong detonation, four equations for the three unknowns  $A_1, A_2, D$ . Therefore, these cases are not evolutionary, and the linear perturbation theory breaks down. This is just a sign of the problems discussed above for these solutions. In contrast, as seen in the left panel of Fig. 6, in the weak detonation case we have three unstable modes behind the wall. Therefore, there are four unknowns, namely,  $A_1, A_2, A_3$ , and  $D$ , and the weak detonation is evolutionary.

### C. Solving the perturbation equations

Let us thus consider a solution of the form  $\vec{A}_+(z) = 0$  for  $z > 0$ , and

$$\vec{A}_-(z) = A_1 \vec{L}_1 e^{q_1 z} + A_2 \vec{L}_2 e^{q_2 z} + A_3 \vec{L}_3 e^{q_3 z} \quad (70)$$

for  $z < 0$ . The junction conditions (49-51), as well as the surface equation (57), require evaluating Eq. (70) at the interface position  $z = \zeta(x^\perp, t)$ . However, to first order in the perturbations, this is equivalent to evaluating at  $z = 0$ . Therefore we have, in front of the wall,

$$\delta v_+ = 0, \quad \delta p_+ = 0, \quad v_+^\perp = 0, \quad (71)$$

and behind the wall (omitting a factor  $e^{\Omega t + i k x^\perp}$ ),

$$\delta v_- = A_1 + A_2 + A_3, \quad (72)$$

$$\delta p_- = -w_- \gamma_-^2 \left[ \frac{\Omega + q_2 v_-}{\Omega v_- + q_2} A_2 + \frac{\Omega + q_3 v_-}{\Omega v_- + q_3} A_3 \right], \quad (73)$$

$$v_-^\perp = \frac{i q_1}{k} A_1 + \frac{i k}{\Omega v_- + q_2} A_2 + \frac{i k}{\Omega v_- + q_3} A_3, \quad (74)$$

On the other hand, for the perturbation of the wall we have (omitting again a factor  $e^{\Omega t + i k x^\perp}$ )

$$\partial_0 \zeta = \Omega D, \quad \partial_\perp \zeta = i k D, \quad \partial_0^2 \zeta = \Omega^2 D, \quad \partial_\perp^2 \zeta = -k^2 D. \quad (75)$$

Inserting Eqs. (71-75) in Eqs. (49-51,57), we obtain a homogeneous system of linear equations for the constants  $A_1, A_2, A_3$  and  $D$ . It is convenient to redefine the unknowns as  $\tilde{A} = (\gamma_-^2 / \gamma_{s-}^2) A_3 / Q_3$ ,  $\tilde{B} = (\gamma_-^2 / \gamma_{s-}^2) A_2 / Q_2$ ,  $\tilde{C} = -\gamma_-^2 A_1$ ,  $\tilde{D} = k D$ , where the quantities  $\gamma_{s-}^2$  and  $Q_{2,3}$  are defined below. After some manipulations, the system of equations can be written in matrix form as (from now on, we use the notation  $k = |k|$ )

$$\begin{bmatrix} -\frac{1}{R} & \frac{1}{R} & \frac{\hat{\Omega}}{v_- \gamma_-^2} & -\Delta v \\ -(1 + \frac{v_- \hat{\Omega}}{R}) & -(1 - \frac{v_- \hat{\Omega}}{R}) & 1 + v_-^2 & (1 - v_- v_+) \frac{\Delta v}{v_+} \hat{\Omega} \\ -(1 + \frac{\hat{\Omega}}{v_- R}) & -(1 - \frac{\hat{\Omega}}{v_- R}) & 2 & \frac{F_{\text{dr}}}{w_+ v_+ \gamma_+^2} (\hat{\Omega}^2 + 1) k d \\ \frac{\gamma_{s-}^3}{\gamma_-^3} Q_3 - \frac{\beta_-}{v_-} P_3 & \frac{\gamma_{s-}^3}{\gamma_-^3} Q_2 - \frac{\beta_-}{v_-} P_2 & \frac{-\gamma_{s-}^3}{\gamma_-^3 \gamma_{s-}^2} & \frac{2}{\gamma_{s-}^2} \left[ \frac{\langle \gamma_\lambda v \rangle}{\gamma_-} (\hat{\Omega}^2 + 1) k d - \left\langle \frac{\gamma_\lambda^3}{\gamma^2} \right\rangle \frac{\hat{\Omega}}{\gamma_-} \right] \end{bmatrix} \begin{bmatrix} \tilde{A} \\ \tilde{B} \\ \tilde{C} \\ \tilde{D} \end{bmatrix} = 0, \quad (76)$$

where we have defined the quantities  $\hat{\Omega} = \Omega / k$ , and

$$\frac{1}{\gamma_{s-}^2} = 1 - \frac{v_-^2}{c_{s-}^2}, \quad R = \sqrt{\frac{\gamma_-^2}{\gamma_{s-}^2} + \frac{\hat{\Omega}^2}{c_{s-}^2}}, \quad P_2 = v_- \pm \frac{\hat{\Omega}}{R}, \quad Q_2 = 1 \pm \frac{v_-}{c_{s-}^2} \frac{\hat{\Omega}}{R}. \quad (77)$$

(notice that, for weak detonations, we have  $\gamma_{s-}^2 < 0$ ). Nontrivial solutions exist if the determinant of the matrix in Eq. (76) vanishes.

Due to the symmetry of the matrix, the  $4 \times 4$  determinant is easy to calculate. Indeed, calling  $\det_{ij}$  the determinant of the  $3 \times 3$  matrix that results by removing the  $i$ -th row and the  $j$ -th column, we find that  $\det_{14} = 0$ , and we have the equation

$$\left[ \frac{F_{\text{dr}} \det_{34}}{w_+ v_+ \gamma_+^2} - \frac{2 \langle \gamma_\lambda v \rangle \det_{44}}{\gamma_{s-}^2} \right] k d (\hat{\Omega}^2 + 1) - \left[ \frac{\Delta v}{v_+} (1 - v_+ v_-) \det_{24} - \left\langle \frac{\gamma_\lambda^3}{\gamma^2} \right\rangle \frac{2 \det_{44}}{\gamma_{s-}^2} \right] \hat{\Omega} = 0. \quad (78)$$

Moreover, all of the  $3 \times 3$  determinants are proportional to

$$\frac{2}{R} \left( 1 - \frac{\hat{\Omega}^2}{v_-^2 \gamma_-^2} \right) \quad (79)$$

Therefore, a solution for  $\Omega > 0$  is given by  $\hat{\Omega} = -\gamma_- v_-$ . For this value of  $\hat{\Omega}$ , we have  $R = \gamma_-$ ,  $P_2 = 0$ ,  $Q_2 = \gamma_{s-}^{-2}$ , and we obtain, from Eq. (76),  $\tilde{B} - \tilde{C} = \tilde{A} = \tilde{D} = 0$ . This gives  $A_1 + A_2 = A_3 = D = 0$ . As a consequence, all the perturbation variables in (72-75) vanish in this case (notice that  $\Omega + q_2 v_- \propto P_2$ ,  $\Omega v_- + q_2 \propto Q_2$ ). Hence, this is a spurious solution, like in the case of deflagrations [20, 21]. Omitting the factor (79), which cancels out in Eq. (78), the determinants are given by

$$\det_{24} = \frac{\gamma_{\lambda-}^3}{\gamma_-^3} \frac{c_{s-}^2 + v_-^2}{c_{s-}^2} - 2\beta_-, \quad \det_{34} = \frac{\gamma_{\lambda-}^3}{\gamma_-^3} v_-^2 \frac{c_{s-}^2 + 1}{c_{s-}^2} - \beta_-(1 + v_-^2), \quad \det_{44} = \frac{1}{\gamma_-^2}. \quad (80)$$

Notice that  $\hat{\Omega}$  does not appear in these expressions. Hence, Eq. (78) gives a simple quadratic equation for  $\Omega$ . The solution is

$$\Omega d = \mathcal{C} \pm \sqrt{\mathcal{C}^2 - (kd)^2}, \quad (81)$$

where the real constant  $\mathcal{C}$  is given by

$$\mathcal{C} = \frac{1}{2|v_-|} \frac{\mathcal{N}}{\mathcal{D}}, \quad (82)$$

with

$$\mathcal{N} = -\frac{1}{\gamma_-} \left\langle \frac{\gamma_{\lambda}^3}{\gamma^2} \right\rangle \frac{v_-^2 - c_{s-}^2}{c_{s-}^2} + \frac{1 - v_+ v_-}{1 - v_-^2} \left[ \beta_- - \frac{\gamma_{\lambda-}^3}{\gamma_-^3} \frac{c_{s-}^2 + v_-^2}{2c_{s-}^2} \right] \frac{\Delta v}{v_+}, \quad (83)$$

$$\mathcal{D} = \frac{\langle \gamma_{\lambda} v \rangle}{\gamma_- v_-} \frac{v_-^2 - c_{s-}^2}{c_{s-}^2} - \frac{1 + v_-^2}{2v_-^2} \left[ \beta_- - \frac{\gamma_{\lambda-}^3}{\gamma_-^3} \frac{1 + c_{s-}^2}{1 + v_-^2} \frac{v_-^2}{c_{s-}^2} \right] \frac{F_{\text{dr}}}{w_-}. \quad (84)$$

The structure of the solutions  $\Omega(k)$  is very simple. For  $kd < |\mathcal{C}|$  we have two real solutions, whereas for  $kd > |\mathcal{C}|$  we have two complex solutions with the same real part. In either case, we have  $\text{Re}(\Omega) > 0$  if, and only if,  $\mathcal{C} > 0$  (see Fig. 7). If this is the case, perturbations at all wavenumbers are unstable. As we discuss below, the constant  $\mathcal{C}$  will take positive as well as negative values in different velocity intervals. For  $\mathcal{C} < 0$ , we have  $\text{Re}(\Omega) < 0$  for all  $k$ . It is important to remember, though, that we are considering perturbations behind the wall, which, for  $\text{Re}(\Omega) < 0$  increase exponentially with the distance from the wall [i.e., correspond to  $\text{Re}(q) < 0$ ] and must be discarded. Since there is also no solution with  $\text{Re}(\Omega) > 0$ , in this case there must be solutions corresponding to undamped oscillations. Studying these solutions, which correspond to  $\text{Re}(\Omega) = \text{Re}(q) = 0$ , is not one of the goals of the present paper. In any case, such solutions with  $\text{Re}(\Omega) = 0$  are marginally stable, and, to determine the stability, one should go beyond linear perturbations.

For completeness, we have also considered perturbations in front of the wall, for which the treatment is very similar. As we have seen, in this case, the solutions which must be discarded are those with  $\text{Re}(\Omega) > 0$ . We found again two solutions of the form (81). Nevertheless, in this case, it can be seen that the stability parameter is always negative.

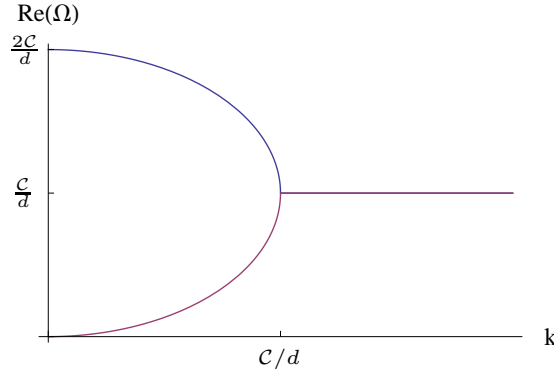


FIG. 7: The real part of  $\Omega$  as a function of  $k$ , for  $\mathcal{C} > 0$ .

This indicates that any perturbation in front of the wall is exponentially stable, as expected physically.

Before going on to the determination of the instability intervals, we wish to compare these results with the deflagration case [20, 21]. In brief, deflagrations with velocities above a critical velocity  $v_c$  are stable under perturbations at any wavelength. Below the velocity  $v_c$ , there is a range of unstable wavenumbers,  $0 < k < k_c$ . Thus, short wavelengths, as well as long wavelengths, are stable. In contrast, for detonations all wavenumbers are either stable or unstable, depending on the wall velocity. It is interesting that the critical velocity  $v_c$  arises due to the dependence of  $\Omega$  on terms which are roughly of the form  $\beta_{\pm} - 1$ . A similar dependence is present in Eqs. (83-84). Indeed, except for the limit  $v_w \rightarrow 1$ , most of the factors in Eqs. (83-84) are  $\sim 1$ , and we may write, roughly,

$$\mathcal{N} \sim -\frac{v_-^2 - c_{s-}^2}{c_{s-}^2} + (\beta_- - 1) \frac{\Delta v}{v_+}, \quad (85)$$

$$\mathcal{D} \sim \frac{v_-^2 - c_{s-}^2}{c_{s-}^2} - (\beta_- - 1) \frac{F_{\text{dr}}}{w_-}. \quad (86)$$

In the deflagration case, the parameters  $\beta_{\pm}$  are critical for stability, since, as we have seen in the previous section, we have roughly  $\beta_{\pm} \sim v_w^2/v_c^2$ . Since  $v_c$  is generally small, for a deflagration the factors  $\beta_{\pm} - 1$  will change sign at  $v_w \simeq v_c$ . In contrast, for weak detonations we generally have  $\beta_- \gg 1$ . In this case, the sign of the numerator  $\mathcal{N}$  will depend essentially on the balance between two parameters characterizing the hydrodynamics, namely,  $(v_-^2 - c_{s-}^2)$  and  $\Delta v$ . On the other hand, the sign of the denominator  $\mathcal{D}$  depends on  $(v_-^2 - c_{s-}^2)$  and  $F_{\text{dr}}$ .

#### IV. STABILITY OF WEAK DETONATIONS

Let us first consider a specific example. In Fig. 8 we plot the value of the stability parameter  $\mathcal{C}$  as a function of  $v_w$ , for the cases considered in the right panel of Fig. 4. For the case of small  $\lambda$ , we have changed the value  $\lambda = 0.2$  of Fig. 4 to  $\lambda = 0$  in order to show the behavior in this limiting case. We see that the curves are qualitatively similar for the three values of  $\lambda$ . Indeed,  $\mathcal{C}$  is positive for the “unphysical” branch of weak detonations discussed in the previous section, and is negative for the “physical” branch, as expected. (We plotted the negative part of the curve in gray dashes to emphasize the fact that  $\mathcal{C} < 0$



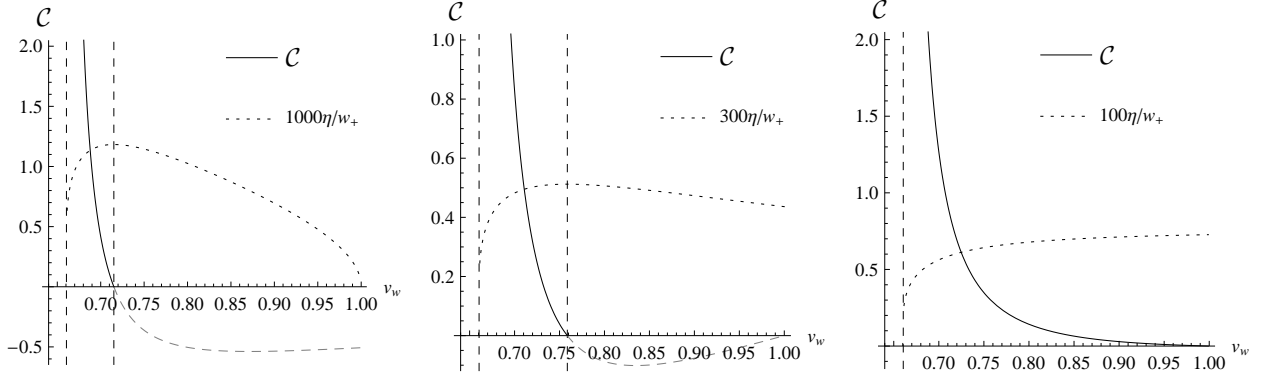


FIG. 8: The stability parameter  $\mathcal{C}$  as a function of  $v_w$ , for the bag model with  $\bar{L} = 0.03$ ,  $T_N/T_c = 0.95$ , and for  $\lambda = 0$  (left),  $\lambda = 1$  (center), and  $\lambda = 5$  (right). The vertical lines indicate the values of  $v_J$  and  $v_{\text{crit}}$ .

actually corresponds to marginal stability.) For a better comparison, we show the curves of  $\eta$  vs  $v_w$  (dotted lines). As is observed, the change of sign of  $\mathcal{C}$  occurs exactly at the velocity  $v_{\text{crit}}$  corresponding to maximum friction  $\eta_{\text{max}}$  [cf. Fig. 4] (we shall check this analytically). Furthermore,  $\mathcal{C}$  (and, thus,  $\Omega$ ) seems to diverge at the Jouguet velocity  $v_J$ . However, the present treatment breaks down near the Jouguet point. Below, we analyze this behavior in detail.

### A. Range of instability

It is easy to see, from Eq. (83), that the numerator  $\mathcal{N}$  will always change sign at the velocity  $v_w = v_{\text{crit}}$ , as observed in Fig. 8. Indeed, notice that the condition for vanishing  $\mathcal{N}$  is the same as Eq. (41) corresponding to the point separating the two branches of solutions. Moreover, from the approximation (85), we see that  $\mathcal{N}$  is negative for  $v_w = 1$  and positive at the Jouguet point, since the quantities  $\Delta v$  and  $v_-^2 - c_{s-}^2$  vanish at these opposite ends of the weak detonation interval (in blue in Fig. 2).

In the limit  $v_w \rightarrow 1$ , the approximation (85) is not valid, since the factors  $\gamma_-^{-1}$  in Eq. (83) vanish. For  $\lambda = 0$ , the gamma factors cancel out. However, for  $\lambda \neq 0$ , both  $\mathcal{N}$  and  $\mathcal{D}$  vanish. Nevertheless, it is not difficult to see that, in this limit, we have  $\mathcal{N} \sim \gamma_-^{-3}$ ,  $\mathcal{D} \sim \gamma_-^{-1}$ . Hence, the parameter  $\mathcal{C}$  vanishes in the limit  $v_w \rightarrow 1$ , as seen in the central and right panels of Fig. 8. This is the only qualitative difference between the cases  $\lambda = 0$  and  $\lambda \neq 0$ , and it does not affect the stability analysis.

Regarding the denominator  $\mathcal{D}$ , it is apparent in Eq. (86) that it has a zero in the weak detonation range. This zero is not at the Jouguet point. Indeed, for  $v_- = -c_{s-}$ , we have  $\mathcal{D} < 0$ . Hence, the divergence of  $\Omega$  does not occur exactly at the Jouguet point, but at a velocity  $v'_{\text{crit}} > v_J$  (see Fig. 9), although this cannot be appreciated in Fig. 8. For  $v_w > v'_{\text{crit}}$  we have  $\mathcal{D} > 0$ , and the sign of the stability parameter  $\mathcal{C}$  is determined by the numerator  $\mathcal{N}$ . As observed in Figs. 8 and 9, the velocity  $v'_{\text{crit}}$  is very close to the Jouguet velocity  $v_J$ . Below we shall see that this is the general case.

Thus, the whole branch of weaker weak detonations ( $v_{\text{crit}} < v_w < 1$ ) corresponds to  $\text{Re}(\Omega) < 0$ . As already discussed, these solutions must be discarded, and we have no solution with  $\text{Re}(\Omega) \neq 0$ . Hence, for this velocity range we have marginal stability and

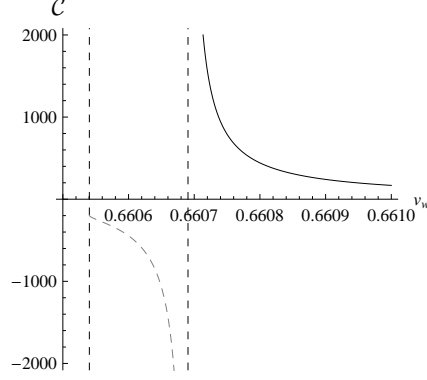


FIG. 9: The same as Fig. 8, zooming in near  $v_w = v_J$ . Vertical dashed lines indicate the values  $v_J$  and  $v'_{\text{crit}}$ .

one should consider non-linear perturbations. Nevertheless, the linear perturbation result suggests that these detonations will be stable. In contrast, detonations in the velocity range  $v'_{\text{crit}} < v_w < v_{\text{crit}}$  are unstable. This constitutes almost the whole branch of stronger weak detonations, since we have  $v'_{\text{crit}} \simeq v_J$ .

It is important to notice that our treatment breaks down for velocities which are too close to the Jouguet point. In the first place, for the unstable solutions on the right of the singularity, the growth rate becomes higher and higher as  $v_w$  approaches  $v'_{\text{crit}}$ . Hence, the small perturbation calculation will break down as the characteristic growth time becomes much shorter than the scale which characterizes the dynamics. This happens for  $\text{Re}(\Omega)^{-1} \ll d$  (equivalently, for  $\mathcal{C} \gg 1$ ). Therefore, the actual value of  $\Omega$  may have a natural cutoff. Nevertheless, even if  $\text{Re}(\Omega)$  does not diverge, we expect a strong instability at  $v_w = v'_{\text{crit}}$ .

For the solutions on the left of the singularity the situation is much less clear. Here, we have  $\text{Re}(\Omega) < 0$ , which means that the linear stability analysis is inconclusive. However, as we have already discussed, the approach of considering perturbations from a constant solution breaks down as we approach the Jouguet point. Therefore, instead of considering non-linear perturbations, one should consider perturbations around the appropriate fluid profile. It is perfectly possible that such a calculation will give linearly unstable modes. This would match smoothly the behavior for  $v_w > v'_{\text{crit}}$ .

We shall now estimate the value of  $v'_{\text{crit}}$  and analyze how close it is to  $v_J$  in the general case. To begin with, we can see, from Eqs. (86) and (85), that  $v'_{\text{crit}}$  is much closer to  $v_J$  than  $v_{\text{crit}}$ . More explicitly, we can see that the corresponding value of  $v_-$  is much closer to  $c_{s-}$ . Indeed, taking into account that  $\beta_- \gg 1$ , we see that  $\mathcal{N}$  vanishes for

$$\frac{|v_-| - c_{s-}}{c_{s-}} \approx \frac{1}{2} \frac{1}{s_-} \left( -\frac{\partial F_{\text{dr}}}{\partial T_-} \right) \frac{\Delta v / v_+}{F_{\text{dr}} / w_-}. \quad (87)$$

while  $\mathcal{D}$  vanishes for

$$\frac{|v_-| - c_{s-}}{c_{s-}} \approx \frac{1}{2} \frac{1}{s_-} \left( -\frac{\partial F_{\text{dr}}}{\partial T_-} \right). \quad (88)$$

Thus, we see that, for the case of  $v_{\text{crit}}$ , the value of  $v_-$  will lie somewhere between  $c_{s-}$  and 1, but cannot be very close to  $c_{s-}$ , since at the Jouguet point we have a maximum  $\Delta v$  and a minimum  $F_{\text{dr}}$ . Moreover,  $F_{\text{dr}} / w_-$  can be very small, since the reheating is maximum

at the Jouguet point<sup>8</sup>. On the other hand, the rhs of Eq. (88) is suppressed by a factor  $(F_{\text{dr}}/w_-)/(\Delta v/v_+)$  with respect to the rhs of Eq. (87). Hence,  $v_-$  will be much closer to  $c_{s-}$  in this case. Consequently,  $v'_{\text{crit}}$  will be much closer to  $v_J$  than  $v_{\text{crit}}$ .

For a given model, we can estimate the value of  $v_-$  corresponding to  $v_w = v'_{\text{crit}}$  from Eq. (88). For the bag EOS, this gives

$$\frac{|v_-| - c_{s-}}{c_{s-}} \approx \frac{1}{2} \frac{L}{w_-} \frac{T_-^2 T_+^2}{T_c^4} \sim \frac{\bar{L}}{2}. \quad (89)$$

Besides, since the Jouguet point is a minimum of  $|v_+|$  vs  $|v_-|$  (see Fig. 2), we have  $|v_+| - v_J \sim (|v_-| - c_{s-})^2$ . Hence, according to Eq. (89), we have

$$v'_{\text{crit}} - v_J \sim (\bar{L}/2)^2. \quad (90)$$

The parameter  $\bar{L}$  is bounded by 1, and in most cases we have  $\bar{L} \ll 1$ . Moreover, a large  $\bar{L}$  hinders the existence of detonations, due to the hydrodynamical obstruction caused by the release of latent heat. As can be observed in Fig. 10 (left panel), detonations cannot exist at all if the latent heat is too large. How large, depends on the amount of supercooling (see Ref. [9]). For the case considered in the figure, i.e., for a supercooling of  $T_N/T_c = 0.9$ , the limit is  $\bar{L} \simeq 0.35$ . This hydrodynamic effect is most important near the Jouguet point, where the reheating is maximum. For large enough latent heat,  $T_-$  surpasses the critical temperature (see Fig. 10, right panel). Moreover, the reheating may cause the driving force to become negative. Of course, this means that such a solution is unreachable, as it would require a negative friction (this can be observed in the left panel of Fig. 10). For the approximation (29), this happens for  $T_- = T_c^2/T_N$ . As a consequence, for large enough latent heat, the velocity  $v'_{\text{crit}}$ , being very close to the Jouguet point, will not be achieved. In the case of Fig. 10, the existence of the Jouguet point requires  $\bar{L} \lesssim 0.15$ . Thus, for the cases where  $v_J$  and  $v'_{\text{crit}}$  exist we have, according to Eq. (90),  $v'_{\text{crit}} - v_J \lesssim 0.005$ .

## B. Bubble expansion, detonations, and runaway walls

As already mentioned, hydrodynamic instabilities may determine, in the case of multiple solutions, which one will be realized during a phase transition. In principle, the fact that a solution is unstable does not imply that it will not be realized. For instance, in the case of an unstable deflagration, the wall is unstable under corrugations on a characteristic scale  $\lambda_c$ , while long wavelengths, as well as short wavelengths, are stable [21, 23, 32]. Thus, a bubble will grow to a size  $\sim \lambda_c$  before these corrugation instabilities can destabilize the wall.

The case of detonations is certainly different. As we have seen, an unstable detonation is unstable at all wavelengths with similar growth rates. As a consequence, such a configuration, if ever formed during bubble expansion, will decay immediately, either to some of the stable configurations, such as a weaker weak detonation, or to a runaway solution. Thus, weak detonations of the lower velocity branch will most likely never be realized in a phase transition. In particular, if the ultra-relativistic friction is small enough, there will be no detonations at all, as in the cases represented in red in Fig. 4.

<sup>8</sup> For instance, for the bag EOS we have  $F_{\text{dr}}/w_- \sim \bar{L}(1 - T_-^2 T_+^2/T_c^4)$ , while, estimating  $\Delta v$  near the Jouguet point we have, from Eqs. (29-34),  $\Delta v \sim \sqrt{\bar{L}}$ . Hence, we have  $F_{\text{dr}}/w_- \ll \Delta v/v_+$ .

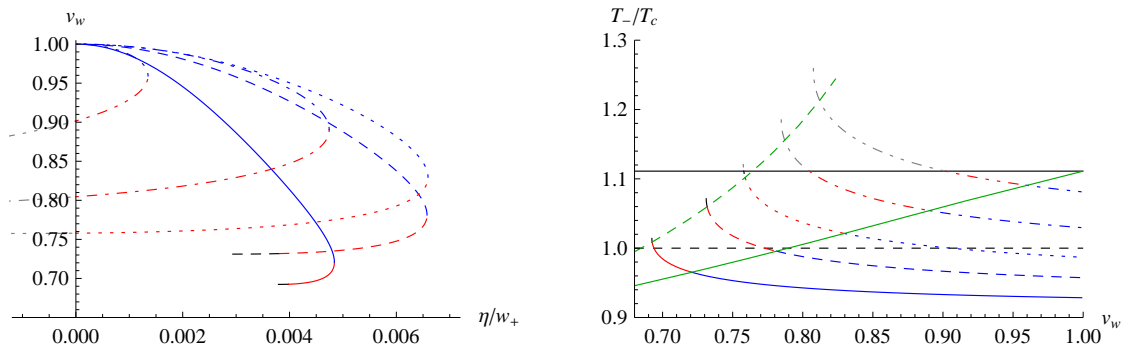


FIG. 10: Left panel: The wall velocity for  $\lambda = 0$  as a function of  $\eta$ , for  $T_N/T_c = 0.9$  and  $\bar{L} = 0.05$  (solid), 0.1 (dashed), 0.15 (dotted), 0.22 (dot-dashed), and 0.3 (dot-dot-dashed). Right panel: The reheating as a function of the wall velocity, corresponding to the curves of the left panel. Blue segments indicate stable solutions and red segments indicate unstable solutions. Black segments indicate the region where our stability analysis breaks down, and grey segments indicate not realizable solutions which require negative values of  $\eta$ . In the right panel, the points corresponding to  $v'_{\text{crit}}$  are indicated by a dashed green line, and those corresponding to  $v_{\text{crit}}$  by a solid green line. The horizontal dashed line indicates the value  $T_- = T_c$ , and the solid line indicates the value  $T_- = T_c^2/T_N$ , for which the driving force vanishes.

As discussed in Sec. II, detonations may coexist with runaway solutions for certain ranges of parameters. For instance, as we decrease the friction parameter  $\eta$ , the runaway solution appears before the stationary solution ceases to exist (see Fig. 4). This raises the question whether the detonation becomes unstable when the runaway solution appears. According to the linear perturbation theory, the answer seems to be no. As discussed above, although inconclusive, the analysis suggests that the detonation solution is stable in the range  $v_{\text{crit}} < v_w < 1$ . There is no reason, thus, for the wall to run away, as long as a detonation solution exists. Indeed, the runaway solution requires highly ultra-relativistic velocities, i.e., an extremely high gamma factor  $\gamma_w$ , while a detonation will most likely have  $\gamma_w \sim 1$ .

### C. Cosmological implications

The unstable growth of a bubble wall may in principle have interesting cosmological consequences. For instance, in the case of deflagrations, instabilities under corrugations of the wall may lead to dendritic growth [23, 33]. Such a complex dynamics may have effects on electroweak baryogenesis [34, 35], magnetic field generation [36], and gravity wave formation [21]. However, the case of unstable detonations is quite different, since large wavelengths are as unstable as short wavelengths. As we have discussed, such detonations will probably not be formed at all, rather than forming and then decaying. Hence, in this case there will not be such interesting effects. On the contrary, any mechanism of relic generation which relies on stronger weak detonation solutions will be negatively affected. Here we discuss a couple of examples.

Being supersonic, detonation fronts are important for the generation of gravitational waves. In this field, a Jouguet detonation has often been assumed for the calculation of the

gravitational wave background from a cosmological phase transition. The Jouguet velocity depends only on thermodynamical parameters and, for a given EOS, is easy to calculate [see, e.g., Eq. (34)]. However, if the friction force is taken into account, the wall velocity will depend also on friction parameters, and the solution will not necessarily be a Jouguet detonation. Moreover, we have argued that this particular solution is quite unlikely. In the first place, due to strong hydrodynamics, the Jouguet velocity may just be unreachable for positive friction. Even if the Jouguet point exists, it corresponds to the lower end of the lower velocity branch of weak detonations, which behaves unphysically as the parameters are varied. Unfortunately, our stability analysis breaks down near the Jouguet point. However, as we have argued, the fact that the growth rate of the instabilities becomes very large near this point suggests that the Jouguet solution is probably unstable as well<sup>9</sup>. We remark, however, that weaker detonations, although causing less disturbances in the fluid, have higher velocities and, hence, may cause stronger gravitational waves (see, e.g., [11]).

An interesting feature of detonations is the fact that the reheating behind the wall may surpass the critical temperature (provided that the latent heat is high enough for the given amount of supercooling). An application of this fact is the interesting idea of supersonic electroweak baryogenesis [37]. In this scenario, small bubbles of the symmetric phase nucleate in the superheated broken-symmetry phase behind the wall. Baryogenesis occurs at the walls of these small bubbles, which move slowly with respect to the fluid. Thus, the necessary conditions for baryogenesis are fulfilled, and the required baryon asymmetry is generated for reasonable values of the parameters, although there are some restrictions. One of them is the fact that the superheating must be strong enough for the symmetric bubbles to fill a sizeable fraction of space.

In this respect, the analysis of Ref. [37] lacks an important feature of bubble growth, namely, the friction force. Indeed, the wall velocity is left as a free parameter, and the temperature  $T_-$  is calculated as a function of  $v_w$ . This is always possible, since the reheating is given exclusively by hydrodynamics. As we have seen, the fluid variables  $T_-, v_-$  only depend on  $T_N$  and  $v_w$  (besides the EOS parameters). In the general case, these relations can be obtained from Eqs. (3-4). For the bag EOS,  $T_-$  and  $v_-$  are given by Eqs. (30) and (31), respectively, as a function of  $v_w$ ,  $T_N/T_c$ , and  $\bar{L}$ . Moreover, a weak detonation profile like that of Fig. 3 will always exist for each wall velocity in the range  $v_J < v_w < 1$ . However, if the velocity is not left as a free parameter but is calculated, this interval will be reduced, due both to physical impossibility and hydrodynamic instabilities. Unfortunately, the reheating is higher for solutions which are closer to the Jouguet point. Therefore, most of the interesting solutions will belong to the unstable branch.

Consider the plots of Fig. 10. The curves of  $T_-$  vs.  $v_w$  (right panel) can be plotted without knowing the friction force. We have  $T_- > T_c$  for wide ranges of values of  $\bar{L}$  and  $v_w$  (namely, all the curves or parts of curves which lie above the horizontal dashed line). However, if we actually calculate the velocity as a function of the friction, we know that a part of each curve (the gray segments) corresponds to velocities which cannot be achieved at all for any positive friction parameter. Besides, another part of each curve corresponds to unstable solutions (the red segments). Only the lower parts of the curves (the blue segments) corresponds to stable detonations. Notice that, in fact, the upper physical bound on  $T_-$  (the horizontal solid line) is never reached for stable solutions, which give values of

---

<sup>9</sup> In any case, we have seen that previous results claiming that the Jouguet detonation is stable [26] are not valid.

$T_-$  below the solid green line. This reduces the region of realizable solutions with  $T_- > T_c$  to the triangular region between this line and the horizontal dashed line.

These restrictions on the reheating will certainly shrink the available parameter space for the supersonic baryogenesis scenario, since the symmetric bubbles need a considerable amount of superheating to nucleate. It is out of the scope of the present work to calculate the nucleation of symmetric bubbles, which would require considering a specific model. In order to appreciate the restriction on the scenario discussed in Ref. [37], we consider, as in that work, the detonation region in the  $(\alpha_N, v_w)$ -plane for the bag EOS<sup>10</sup>, for  $\bar{L} = 0.15$  (see Fig. 11). Here, the variable  $\alpha_N = L/(4aT_N^4)$  is the same as the variable  $\alpha$  defined in Eq. (33) (since for detonations we have  $T_+ = T_N$ ). Thus, the left panel of Fig. 11 coincides with Fig. 3 of Ref. [37]. The region in white corresponds to detonations for which the reheating exceeds the critical temperature. We see that solutions with higher values of  $T_-$  are closer to the Jouguet point.

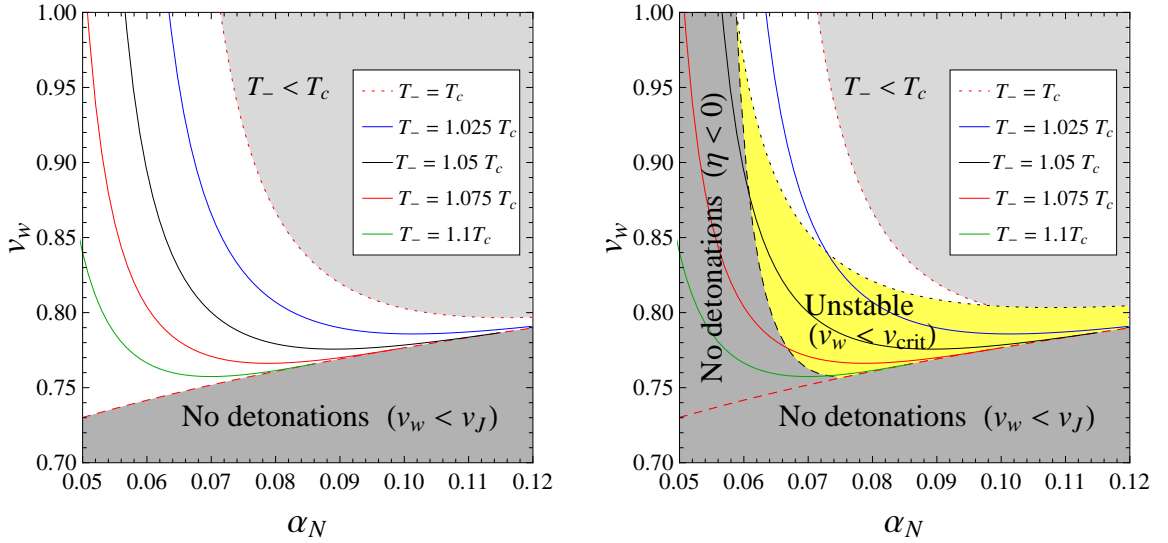


FIG. 11: Region in the  $(\alpha_N, v_w)$ -plane for which  $T_- > T_c$ , for  $\bar{L} = 0.15$ . The red dashed line corresponds to  $v_w = v_J$ . In the right panel, the black dashed line corresponds to solutions with  $\eta = 0$ , and the black dotted line corresponds to  $v_w = v_{\text{crit}}$ .

In the right panel of Fig. 11, we have incorporated the restrictions arising from the calculation of  $v_w$  and from the stability analysis. We considered the case  $\lambda = 0$ , which is the most favorable for detonations (for non-vanishing  $\lambda$ , runaway solutions appear and detonations get reduced to smaller regions of parameter space). We see that the region corresponding to  $T_- > T_c$  is significantly reduced, since most of the detonations in this region are unphysical or unstable. Notice that the region corresponding to  $T_- < T_c$  is also affected, but the reduction of parameter space in this case is insignificant. This can be appreciated already in the right panel of Fig. 10.

<sup>10</sup> In the notation of Ref. [37], we have  $a_+ \equiv a$ ,  $a_- \equiv a(1 - \bar{L})$ , and the value  $\bar{L} = 0.15$  corresponds to  $a_-/a_+ = 0.85$ .

## V. CONCLUSIONS

The possible cosmological consequences of a first-order phase transition depend on the dynamics associated to the motion of bubble walls. It is well known that several hydrodynamic solutions are in principle possible for the propagation of these phase-transition fronts. In particular, for the steady state motion we may have weak or Jouguet detonations, as well as weak, Jouguet or strong deflagrations. Nevertheless, some of these solutions are in fact unstable. The stability analysis is thus important in order to determine which of the propagation modes will be actually realized in a phase transition.

In this work we have studied the stability of detonations under small perturbations of the fluid and the interface. This paper is a sequel of a similar study for the case of deflagrations [21]. The treatment of detonations is quite simpler, due to the fact that the incoming fluid (in the reference frame of the wall) is supersonic. Thus, the fluid in front of the wall is not affected by the phase-transition front. This has two practical consequences for the calculation. On the one hand, for the stationary case, the incoming fluid velocity is given by the wall velocity,  $v_+ = -v_w$ , and the temperature in front of the wall is given by the boundary condition  $T_+ = T_N$ . On the other hand, perturbations originated at the wall cannot grow in front of it. This simplifies the treatment of the stability, since only perturbations of the outgoing fluid must be considered (i.e., perturbations which vanish in front of the wall) [25]. These simplifications allowed us to obtain analytical and model-independent results.

Before the stability analysis, we have discussed in detail the detonation solutions. It is well known that strong detonations are hydrodynamically forbidden [18]. Weak detonations can exist in the velocity range  $v_J < v_w < 1$ , while the Jouguet detonation corresponds to the case  $v_w = v_J$ . The Jouguet velocity  $v_J$  depends on the parameters of the equation of state, and is only determined by the temperature  $T_N$ . However, the precise value of  $v_w$  within this interval will be determined by the balance of the driving and friction forces, and will further depend on friction parameters. Due to strong hydrodynamic effects, it turns out that some velocities in this range may not be realized. Besides, the resulting velocity turns out to be a double valued function of the parameters, and the bubble wall will need to “choose” which of the two possible hydrodynamic configurations to adopt.

Thus we have two branches of weak detonation solutions. One of them, with velocities in the range  $v_{\text{crit}} < v_w < 1$ , where  $v_{\text{crit}}$  is given by Eq. (41), corresponds to weaker weak detonations. The other branch has velocities in the range  $v_J < v_w < v_{\text{crit}}$  and corresponds to stronger weak detonations. This branch behaves rather unphysically with the parameters. Although weak detonations are generally believed to be stable [20], numerical simulations [24] suggest that these stronger solutions are not.

We have applied the standard stability analysis for fluid interfaces [22] to the case of relativistic detonation fronts in a phase transition. We have pointed out that this analysis breaks down at the Jouguet point. This is because the approach considers perturbations around constant velocity and temperature, which is not the case of the Jouguet detonation profile. As a consequence, previous results on the stability of Jouguet detonations [25, 26] are not valid. We have shown that weak detonations of the lower velocity branch are generally unstable under linear perturbations at all wavelengths. More specifically, weak detonations are unstable in the range  $v'_{\text{crit}} < v_w < v_{\text{crit}}$ , where  $v'_{\text{crit}}$  is roughly given by Eq. (88). Below  $v'_{\text{crit}}$ , our approach breaks down. Nevertheless, as we have seen,  $v'_{\text{crit}}$  is very close to the Jouguet velocity  $v_J$ . Therefore, it is quite unlikely that the actual value of the wall velocity (taking into account the friction) will fall in this very small interval. Regarding the higher

velocity branch, the linear perturbation analysis is not conclusive, but we have argued that these solutions will probably be stable. This means that, in the case of coexistence of a detonation and a runaway solution, it is the stationary solution the one which will be realized.

Our main result is, thus, that the branch of weak detonations which are closer to the Jouguet point will not be realized during a phase transition. Unfortunately, these solutions are cosmologically interesting due to their strong disturbance of the fluid. We have discussed, in particular, how our results affect a mechanism of electroweak baryogenesis with detonation walls [37]. This mechanism is based on the fact that the reheating behind the wall may exceed the critical temperature, allowing the nucleation of symmetric-phase bubbles in the superheated fluid inside the broken-symmetry bubbles. The regions in parameter space for this scenario are significantly reduced once unstable detonations are discarded.

### Acknowledgements

This work was supported by Universidad Nacional de Mar del Plata, Argentina, grant EXA 607/12.

- 
- [1] For recent works, see, e.g., C. Caprini, R. Durrer and G. Servant, Phys. Rev. D **77**, 124015 (2008) [arXiv:0711.2593 [astro-ph]]; S. J. Huber and T. Konstandin, JCAP **0809**, 022 (2008) [arXiv:0806.1828 [hep-ph]]; S. J. Huber and T. Konstandin, JCAP **0805**, 017 (2008) [arXiv:0709.2091 [hep-ph]]. A. Megevand, Phys. Rev. D **78** (2008) 084003 [arXiv:0804.0391 [astro-ph]]; T. Kahniashvili, L. Kisslinger and T. Stevens, Phys. Rev. D **81**, 023004 (2010) [arXiv:0905.0643 [astro-ph.CO]]. J. Kehayias and S. Profumo, JCAP **1003**, 003 (2010) [arXiv:0911.0687 [hep-ph]]; J. M. No, Phys. Rev. D **84**, 124025 (2011) [arXiv:1103.2159 [hep-ph]]; L. Leita, A. Megevand and A. D. Sanchez, JCAP **1210**, 024 (2012) [arXiv:1205.3070 [astro-ph.CO]]; M. Hindmarsh, S. J. Huber, K. Rummukainen and D. J. Weir, Phys. Rev. Lett. **112**, 041301 (2014) [arXiv:1304.2433 [hep-ph]].
  - [2] For a review, see D. Grasso and H. R. Rubinstein, Phys. Rept. **348**, 163 (2001) [arXiv:astro-ph/0009061].
  - [3] A. Vilenkin and E.P.S. Shellard, *Cosmic Strings and Other Topological Defects* (Cambridge University Press, Cambridge, England, 1994); A. Vilenkin, Phys. Rept. **121**, 263 (1985).
  - [4] For reviews, see A. G. Cohen, D. B. Kaplan and A. E. Nelson, Ann. Rev. Nucl. Part. Sci. **43**, 27 (1993) [arXiv:hep-ph/9302210]; A. Riotto and M. Trodden, Ann. Rev. Nucl. Part. Sci. **49**, 35 (1999) [arXiv:hep-ph/9901362].
  - [5] E. Witten, Phys. Rev. D **30**, 272 (1984); G. M. Fuller, G. J. Mathews and C. R. Alcock, Phys. Rev. D **37**, 1380 (1988); J. H. Applegate and C. J. Hogan, Phys. Rev. D **31**, 3037 (1985); H. Kurki-Suonio, Phys. Rev. D **37**, 2104 (1988); J. Ignatius, K. Kajantie, H. Kurki-Suonio and M. Laine, Phys. Rev. D **50**, 3738 (1994) [arXiv:hep-ph/9405336].
  - [6] A. F. Heckler, Phys. Rev. D **51** (1995) 405 [arXiv:astro-ph/9407064];
  - [7] A. Megevand and F. Astorga, Phys. Rev. D **71**, 023502 (2005) [hep-ph/0409321].
  - [8] See, e.g., M. Gyulassy, K. Kajantie, H. Kurki-Suonio and L. D. McLerran, Nucl. Phys. B **237**, 477 (1984); H. Kurki-Suonio, Nucl. Phys. B **255**, 231 (1985); K. Kajantie and H. Kurki-Suonio,



- Phys. Rev. D **34**, 1719 (1986); K. Enqvist, J. Ignatius, K. Kajantie and K. Rummukainen, Phys. Rev. D **45**, 3415 (1992).
- [9] A. Megevand and A. D. Sanchez, Nucl. Phys. B **820**, 47 (2009) [arXiv:0904.1753 [hep-ph]].
  - [10] J. R. Espinosa, T. Konstandin, J. M. No and G. Servant, JCAP **1006**, 028 (2010) [arXiv:1004.4187 [hep-ph]];
  - [11] L. Leita0 and A. Megevand, Nucl. Phys. B **844**, 450 (2011) [arXiv:1010.2134 [astro-ph.CO]].
  - [12] T. Konstandin and J. M. No, JCAP **1102**, 008 (2011) [arXiv:1011.3735 [hep-ph]].
  - [13] A. Megevand and A. D. Sanchez, Nucl. Phys. B **865**, 217 (2012) [arXiv:1206.2339 [astro-ph.CO]].
  - [14] See, e.g., M. Dine, R. G. Leigh, P. Y. Huet, A. D. Linde and D. A. Linde, Phys. Rev. D **46**, 550 (1992) [arXiv:hep-ph/9203203]; B. H. Liu, L. D. McLerran and N. Turok, Phys. Rev. D **46**, 2668 (1992). N. Turok, Phys. Rev. Lett. **68**, 1803 (1992); S. Y. Khlebnikov, Phys. Rev. D **46**, 3223 (1992); P. Arnold, Phys. Rev. D **48**, 1539 (1993) [arXiv:hep-ph/9302258]; G. D. Moore and T. Prokopec, Phys. Rev. D **52**, 7182 (1995) [arXiv:hep-ph/9506475]; Phys. Rev. Lett. **75**, 777 (1995) [arXiv:hep-ph/9503296]; P. John and M. G. Schmidt, Nucl. Phys. B **598**, 291 (2001) [Erratum-ibid. B **648**, 449 (2003)]; G. D. Moore, JHEP **0003**, 006 (2000).
  - [15] D. Bodeker and G. D. Moore, JCAP **0905**, 009 (2009) [arXiv:0903.4099 [hep-ph]].
  - [16] S. J. Huber and M. Sopena, arXiv:1302.1044 [hep-ph].
  - [17] A. Megevand, JCAP **1307**, 045 (2013) [arXiv:1303.4233 [astro-ph.CO]].
  - [18] P. J. Steinhardt, Phys. Rev. D **25**, 2074 (1982).
  - [19] M. Laine, Phys. Rev. D **49**, 3847 (1994) [arXiv:hep-ph/9309242].
  - [20] P. Y. Huet, K. Kajantie, R. G. Leigh, B. H. Liu and L. D. McLerran, Phys. Rev. D **48**, 2477 (1993) [arXiv:hep-ph/9212224].
  - [21] A. Megevand and F. A. Membiela, arXiv:1311.2453 [astro-ph.CO].
  - [22] L. D. Landau and E. M. Lifshitz, *Fluid Mechanics* (Pergamon Press, New York, 1989).
  - [23] B. Link, Phys. Rev. Lett. **68**, 2425 (1992).
  - [24] J. Ignatius, K. Kajantie, H. Kurki-Suonio and M. Laine, Phys. Rev. D **49**, 3854 (1994); H. Kurki-Suonio and M. Laine, Phys. Rev. D **51**, 5431 (1995) [arXiv:hep-ph/9501216]; H. Kurki-Suonio and M. Laine, Phys. Rev. D **54**, 7163 (1996) [hep-ph/9512202].
  - [25] M. Abney, Phys. Rev. D **49**, 1777 (1994) [astro-ph/9305021].
  - [26] L. Rezzolla, Phys. Rev. D **54**, 1345 (1996) [astro-ph/9605033].
  - [27] M. Quiros, arXiv:hep-ph/9901312.
  - [28] A. H. Guth and E. J. Weinberg, Phys. Rev. D **23**, 876 (1981).
  - [29] A. D. Linde, Nucl. Phys. B **216**, 421 (1983) [Erratum-ibid. B **223**, 544 (1983)]; Phys. Lett. B **100**, 37 (1981).
  - [30] G. W. Anderson and L. J. Hall, Phys. Rev. D **45**, 2685 (1992).
  - [31] A. Mégevand, Int. J. Mod. Phys. D **9**, 733 (2000) [hep-ph/0006177]; A. Megevand, Phys. Rev. D **64**, 027303 (2001) [hep-ph/0011019]; A. Megevand, Phys. Rev. D **69**, 103521 (2004) [hep-ph/0312305]; A. Megevand and A. D. Sanchez, Phys. Rev. D **77**, 063519 (2008) [arXiv:0712.1031 [hep-ph]]; A. Megevand and A. D. Sanchez, Nucl. Phys. B **825**, 151 (2010) [arXiv:0908.3663 [hep-ph]].
  - [32] K. Kajantie, Phys. Lett. B **285**, 331 (1992).
  - [33] K. Freese and F. C. Adams, Phys. Rev. D **41**, 2449 (1990).
  - [34] M. Kamionkowski and K. Freese, Phys. Rev. Lett. **69**, 2743 (1992) [hep-ph/9208202].
  - [35] M. Abney, Phys. Rev. D **55**, 582 (1997) [hep-ph/9606476].
  - [36] G. Sigl, A. V. Olinto and K. Jedamzik, Phys. Rev. D **55**, 4582 (1997) [astro-ph/9610201].

- [37] C. Caprini and J. M. No, JCAP **1201**, 031 (2012) [arXiv:1111.1726 [hep-ph]].